U.PORTO

FEUP FACULDADE DE ENGENHARIA UNIVERSIDADE DO PORTO

Fraunhofer IWS

M 2022

EVALUATION OF THE COMBINATION OF WIRE AND POWDER FEEDSTOCK FOR THE RESOURCE EFFICIENT MANUFACTURE OF METAL MATRIX COMPOSITE COATINGS VIA LASER CLADDING

MATEUS FRIAS AUGUSTO AZEVEDO PINTO

MASTER'S THESIS SUBMITTED TO FACULDADE DE ENGENHARIA DA UNIVERSIDADE DO PORTO

UNIVERSITY SUPERVISOR
Elsa Wellenkamp de Sequeiros

FRAUNHOFER SUPERVISOR
Maria Manuel Barbosa

September 2022

U.PORTO

FEUP FACULDADE DE ENGENHARIA
UNIVERSIDADE DO PORTO

CANDIDATO	Mateus Frias Augusto Azevedo Pinto		Código: 201706633
TÍTULO	*Evaluation of the combination of wire and powder feedstock for the resource efficient manufacture of Metal Matrix Composite coatings via laser cladding*		
DATA	23 de Setembro de 2022		
LOCAL	Faculdade de Engenharia da Universidade do Porto, F106		
JÚRI	Presidente	Sónia Luisa dos Santos Simões	DEMM - FEUP
	Arguente	Ana Rosanete Lourenço Reis	DeMec- FEUP
	Orientador	Elsa Wellenkamp de Sequeiros	DEMM - FEUP

Resumo

O aumento da oferta comercial de lasers de díodo industriais com maior potência de laser, tornou o revestimento a laser num dos métodos mais eficientes de revestimento de componentes metálicos, devido ao aumento das taxas de deposição de material. Revestimentos de Inconel 625 em fio, reforçados com carboneto de tungsténio em pó, foram produzidos durante este trabalho. O bocal COAXquattro, criado no Fraunhofer IWS, foi utilizado para a produção das amostras estudadas. A variação dos parâmetros de processamento foi usada no estudo da qualidade dos revestimentos, bem como da dissolução do carboneto de tungsténio no compósito. Foram feitos outros ensaios, relativos à diluição do revestimento, microestrutura do compósito, dureza, e resistência ao desgaste. As melhores propriedades mecânicas foram obtidas com a combinação de 60% de WC no compósito, 12100 W (potência do laser), 1400 mm/min. (velocidade transversal), e grau de sobreposição de cordões de 30%. A diferença pouco significativa entre as propriedades medidas desta amostra, e as restantes propriedades estudadas, diz que, para os parâmetros de processamento testados, não é economicamente viável aumentar o teor de carboneto de tungsténio até essa percentagem. Ainda não foi possível atingir cordões sem fissuras, com carboneto de tungsténio não dissolvido e homogeneamente distribuído na matriz.

Palavras-chave

Laser Cladding; Revestimentos em compósito de matriz metálica; COAXquattro; Inconel 625; Carboneto de Tungsténio

Abstract

The increasing availability of industrial diode lasers with higher laser power made laser cladding one of the most efficient methods for coating metallic components, due to the enhanced material deposition rates. Claddings of Inconel 625 wire, reinforced with powder tungsten carbide, were conducted during this work. Fraunhofer IWS's COAXquattro nozzle was used for specimens' production. The variation of processing parameters was employed to study the quality of the coatings, and carbide dissolution in the composite. Further testings were made, regarding dilution of the coating, microstructure of the composite, hardness, and wear resistance. The best mechanical properties were achieved with the combination of 60% WC in the composite, 12100 W (laser power), 1400 mm/min. (transverse speed), and 30% overlap degree. The low gap between this sample's measured properties, and the rest of the studied ones, tells that, for the tested processing parameters, it is not economically viable to increase the tungsten carbide content, up to that percentage. Crack-free clads, with unmelted and homogeneously distributed tungsten carbide in the matrix, still was not accomplished.

Keywords

Laser Cladding; MMC Coatings; COAXquattro; Inconel 625; Tungsten Carbide

Contents

List of Figures

List of Tables

Abbreviations

DMD	Direct Metal Deposition
EBSD	Electron Backscatter Diffraction
EDS	Energy Dispersive X-ray Spectroscopy
HAZ	Heat Affected Zone
IWS	Institut für Werkstoff und Strahltechnik
LC	Laser Cladding
MMC	Metal Matrix Composites
PA	Flat Position
PB	Horizontal Vertical Position
PC	Horizontal Position
SEM	Scanning Electron Microscopy
TCP	Topologically Close Packed
XRD	X-Ray Diffraction

Chapter 1

Introduction

Metal matrix composite coatings have long been used to enhance wear and corrosion resistance of components **[1].** One particular production route that has been gaining popularity in the world of coatings is laser cladding. This technology is the newest and most efficient method for coating metallic surfaces, to improve or recondition components. This is due to the increased availability of industrial diode lasers with much higher laser power, elevating the coating material deposition rate **[2]**. The process can be performed using either wire or powder as feedstock, with each of these having their own advantages when compared to one another **[3].** During the last few years, Dresden's Fraunhofer IWS has been testing the possibility of simultaneously processing powder and wire, to have the best of both worlds, having developed the COAXquattro nozzle **[4]**. The goal for this study is to evaluate the manufacturing efficiency of MMC coatings using the COAXquattro nozzle, while combining Inconel 625 wire with tungsten carbide powder. Specimen production was conducted in Fraunhofer IWS's facilities, varying the LC processing parameters such as tungsten carbide percentage in the composite, laser power, transverse speed and overlap degree. Further studies concerning dilution, microstructure, and mechanical properties, took place in Faculdade de Engenharia da Universidade do Porto. In the end, it is expected to take illations regarding the combination of the varied processing parameters, and how it helped to achieve crack-free clads with unmelted, and homogeneously distributed, reinforcing hard particles in the matrix.

Chapter 2

State of the art

2.1. MMC Coatings

Many engineering components require superior surface properties to meet demanding operating environments. One common approach to improving wear resistance is the addition of coatings to the component's surface. These coatings can be composed of hard particles. Combining carbides or oxides with a metallic binder to form a metal matrix composite (MMC) coating offers multiple advantages. Their unique microstructure allows the coating to withstand high tensile and compressive stresses by the transfer and distribution of the applied load from the ductile matrix to the reinforced hard phase while at the same time offering high resistance to abrasive wear **[5]**. These coatings are regularly found in aviation, aerospace, energy, automotive, and medical industries **[6]**. Figure 1 showcases some common uses for this type of coatings, such as end mills and brake discs. Even though the global impact of the pandemic made the worldwide coating market witness a decline of 3.4 % in 2020, as opposed to the growing trend that the market had from 2017-2019, it is projected to grow from $12.9 billion in 2021, to $21.2 billion in 2028, with the Asia-Pacific region being the major key player **[7].**

Figure 1 - Examples of Metal matrix composite coatings applications **[6].**

2.2. MMC Production

There are various processes and materials used to produce MMCs. A particular production route selection depends on several factors, such as property requirements, final application, and production costs. Oftentimes different production methods for the same constituents lead to completely different characteristics **[1,8,9].** In proper process selection weighs the need for minimising dispersed material damage, preserving strength and promoting wetting and bonding between the different phases. The dispersed phase can be either created *in situ* (within the matrix), typically by an exothermic chemical reaction **[10]** or introduced as an *ex-situ* phase, synthesised separately before being inserted into the matrix **[11]**. In general, *in situ* provides a more homogeneous distribution of the dispersed phase particles, leading to better bonding between the particle and matrix. This results in better mechanical properties and less degradation in high temperature applications, while being cost-effective and scalable. The main problem is that this type of processing is limited to thermodynamically stable materials **[12]**. *Ex situ* processing enables the production of bulk materials that exhibit isotropic characteristics with relative ease and low production cost. However, this processing type has limitations regarding the dispersed material's wettability, leading to difficulty in its incorporation homogeneously within the matrix. Van der Waals and electrostatic forces widely cause this in the liquid mixing process, which leads to particle agglomeration and clustering **[13,14]**. The state of matter also plays its role as processes can be either conducted in a solid or liquid state. Solid state processes combine high temperature with pressure, being known for increasing wettability, reducing segregation effects, and forming brittle reaction, resulting in better mechanical properties. These processes are used for high melting point matrixes **[15,16].** In comparison to solid state, liquid state processes are relatively simple and cost-effective, allowing the formation of dense matrixes and near net-shaped components in complex geometries at relatively high speed **[15,17]**. The dispersed material is blended into a molten metal matrix, which undergoes solidification. Composite properties can be affected by forming a brittle interfacial layer; the control of this parameter is central to obtaining a homogeneous distribution **[17,18]**.

Even though other powder metallurgy processes and casting techniques present most of the processes used for MMC coatings, laser cladding has been showing signs of growth as it is the newest and most efficient method of coating metallic surfaces to improve or recondition components to enhance wear and corrosion resistance, due to the increased availability of industrial diode lasers with much higher laser power, increasing coating material deposition rate **[2]**. The graph displayed in Figure 2 emphasises the reduction in production costs and, most importantly, the exponential increase of productivity that fuels the evolution of the use of the laser cladding technology with expanded laser powers, using the case study of the Inconel 625 alloy.

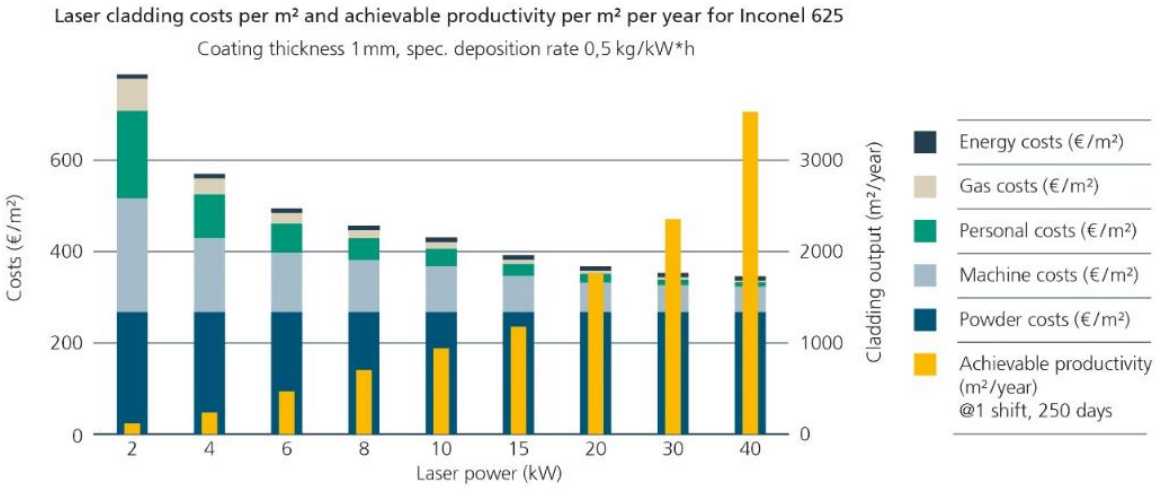

Figure 2 - Laser cladding costs and achievable productivity per m^2/year for Inconel 625, taken from **[19].**

2.3. Laser Cladding Process

The laser cladding method, which can be classified using the already approached terminology as an *in situ* liquid state process, includes a laser beam that melts the powder material injected into a melt pool on the surface of the substrate. The beam is passed through a laser optical fibre into the processing head, composed of the collimation lens, deflecting mirrors, focusing lens and nozzle. The coating material is fed into the processing site and melted by the high energy input. The machine head travels along the desired geometry **[20,21]**. The result is a fully dense, metallurgically bonded coating **[22].** Figure 3 depicts the principle of this technology. This process has been developed in recent years due to its high-energy density and solidification rates, less heat effect on the substrate, minimal dilution, better metallurgical bonding, little distortion in clad geometry, fewer crack openings and flexibility for automation. Furthermore, it produces clads with non-equilibrium microstructures and better surface properties such as corrosion, oxidation, and wear resistance. Due to the high solidification rates of the cladding, it is possible to obtain hard phases with ultra-fine microstructure **[23]**. To prevent welding defects in the clads, a protective gas may be used in the nozzle to cover the effects of oxygen and nitrogen in the cladding atmosphere and obtain a densified bonding. The most used gases are argon and helium **[24]**.

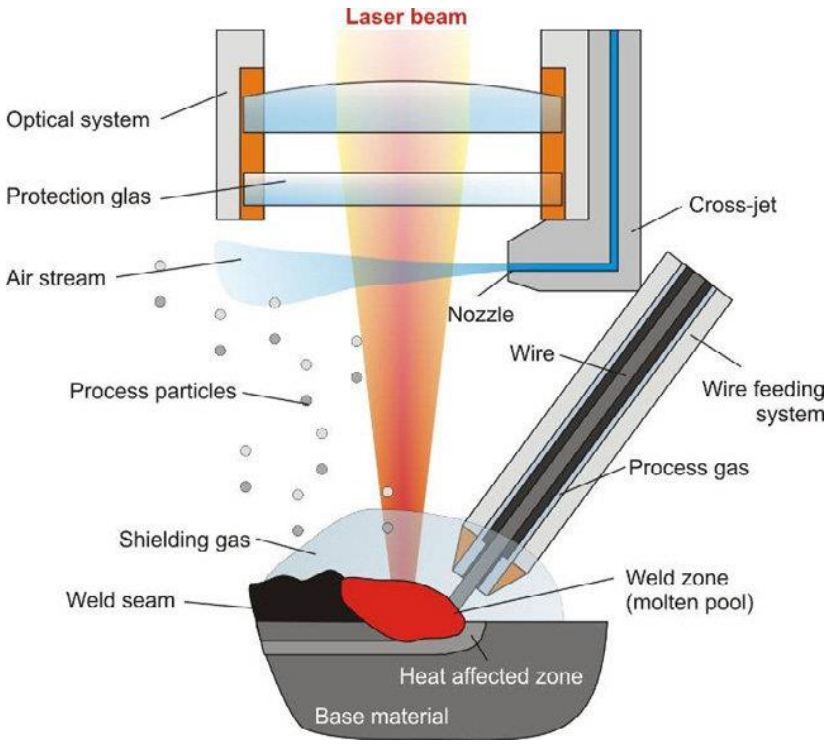

Figure 3 - Principle of the laser cladding process.

The three most relevant parameters are laser power (W), transverse speed (mm/min), and material feed rate (g/min). In addition, the quality of the clad is also dependent on the characteristics of the carrier and shielding gases, the powder size, the laser spot, and the tilt angle of the substrate **[3]**. Metal matrix composites are generally produced using carbides as feeding material. The goal is to keep them intact with minimal dissolution while melting only the matrix. Providing that the difference in melting temperatures of the matrix and the carbides is high enough, this phenomenon can be achieved by processing with laser cladding due to its low heat input **[20].** The process can be performed using different feedstocks, being wire and powder the most used ones. Laser cladding can be classified into two categories: powder feeding cladding system and wire feeding cladding**.** Although the most used feeding material is powder, because of the technical robustness and easy adjustability of the process, it does not have a complete utilisation rate as part of the added powder is not used in the cladding. Furthermore, it is harmful to the handler's respiratory tract, so extra precautions regarding storing and handling must be taken to avoid any possible hazards **[3].** In contrast, the wire feeding method has the advantages of high efficiency, production of superior clad surfaces and total material usage, being at the same time less expensive and environmentally friendly **[25,26].** However, when cladding with wire, it is critical to accurately place it with respect to the melt pool: to be completely melted by the pool's heat, it must be fed directly. Without this assurance, clad quality degradation can happen due to falling drops of material that was melted before reaching the melt pool surface **[27].** Table 1 summarises the main differences between the two types of used feedstock.

Table 1 - Comparison between wire and powder laser deposition at the Fraunhofer IWS, adapted from **[28].**

Filler material	**Wire**	**Powder**
Utilisation rate	100 %	85-95%
Deposition rate	up to 2 kg/h	up to 22 kg/h
Laser power	up to 6 kW	up to 20 kW
Development status	industrial application	industrial application
Cladding position	PA, PB, PC	PA, PB, PC
Laser beam focus	Ø 0.8 - 4 mm	E.g. Ø 30 µm - 50 x 5 mm2
Filler metal dimensions	E.g. Ø 0.4 – 1.6 mm	10 - 200 µm (grain fractions)

Laser powder cladding can be conducted using an either lateral or coaxial deposition. The first one has been falling out of use as the deposited layer of material is restricted to a single line **[29, 30]**. This technique evolved into the injection of the feeding material utilising a nozzle with coaxial configuration: this update allowed for the powder stream's focus point to be at the level of the melt pool, which translated into overall better feeding efficiency **[31]**. In coaxial feeding, while using a ring slit nozzle, Figure 4a, the powder stream tapers along with the laser beam. This flow is guided into a ring-shaped chamber inside the injector, where the coating material will homogeneously leave the injector **[29, 32]**. Coaxial feeding can also be conducted with multiple powder stream nozzles, where the material is injected around the laser beam and converges into a single powder stream focus, Figure 4b. A gas flow is formed around the laser beam so that the powder is distributed homogeneously to achieve appropriate bonding. The quality of the bond depends on the angle of each flow, shape, and diameter of the injector tip **[33]**. This type of injection allows the deposition with higher laser power (>2000 W), increasing productivity **[32, 33]**.

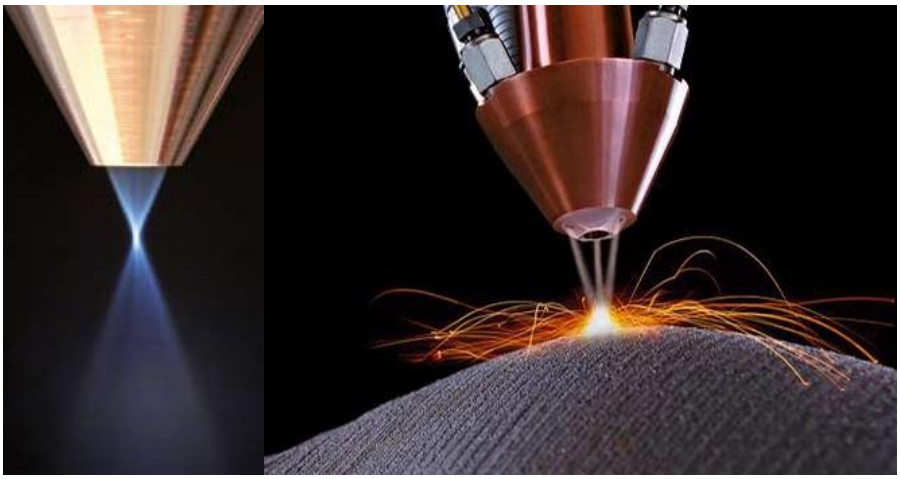

Figure 4 - a) Ring slit nozzle coaxial laser powder cladding; b) Multiple powder stream coaxial laser powder cladding.

Regarding laser wire cladding, the coating can be conducted using flat, horizontal, and vertical positions **[34]**. The geometry of the cladding layer is directly dependent on the wire feeding angle **[35].** Feeding the wire sideways has shown inconsistent results due to the high laser reflection rate from the wire surface. This unbalanced heat transfer makes the wire easily bend and jump out of the molten pool during the process **[36]**. Several methods have been developed to make the wire feed vertically in the middle of lasers to the substrate to solve these problems, such as creating the processing optic COAXwire. With this Fraunhofer IWS' solution, the collimated beam of an up to 4 kW fibre or disc laser is symmetrically split into three partial beams and focused on a circular spot, which coincides with the axis of the wire supply. Thus, the wire directly meets the laser-induced melt bath's centre. Figure 5 shows a schematic representation of this concept. The problem with this technology is that the low achievable values of laser powder generate low material deposition rates, compromising the industrial viability of the process **[37].**

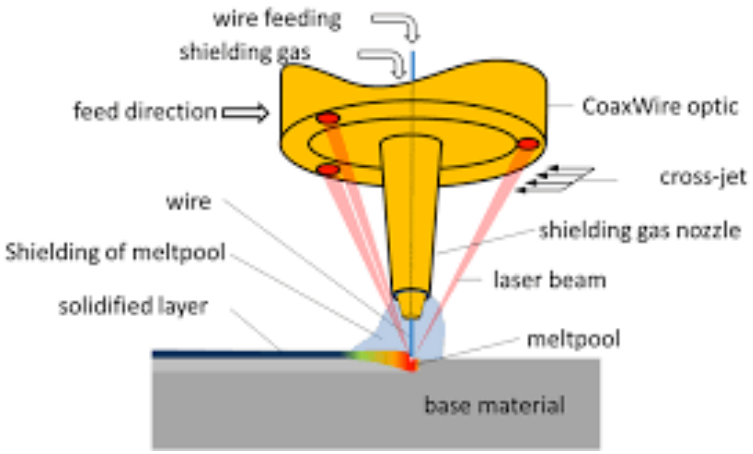

Figure 5 - Coaxial laser wire cladding representation **[38]**.

2.3.1 COAXquattro

The success of the coating depends on the correct choice of technique, feedstock and analysis of the advantages brought. On the one hand, laser powder cladding enables high deposition rates but fails to achieve total feedstock usage. On the other hand, laser wire cladding is limited to low laser power values but tends to be cheaper, has nearly complete deposition efficiency and does not present handling and storage problems. During the last few years, Dresden's Fraunhofer IWS has been testing the possibility of simultaneously processing powder and wire to get the best of both worlds, having developed the COAXquattro nozzle. The mechanism of splitting the beam, utilised previously in COAXwire, was abandoned, and the idea of the totality of the laser being applied centrally was revisited. Figure 6 shows a schematic representation of the nozzle. This new technology has four different wire feeders placed coaxially in the nozzle plus four other powder channels, enabling cladding rates of around 18 kilograms per hour while utilising laser power of up to 20 kW. Systems equipped in this way achieve productivity rates previously reserved only for powder-based laser cladding. Different materials can be fed as required through four-wire and powder channels, enabling *in situ* composite production. In addition, the comparatively short processing times reduce the overall operating costs **[4].**

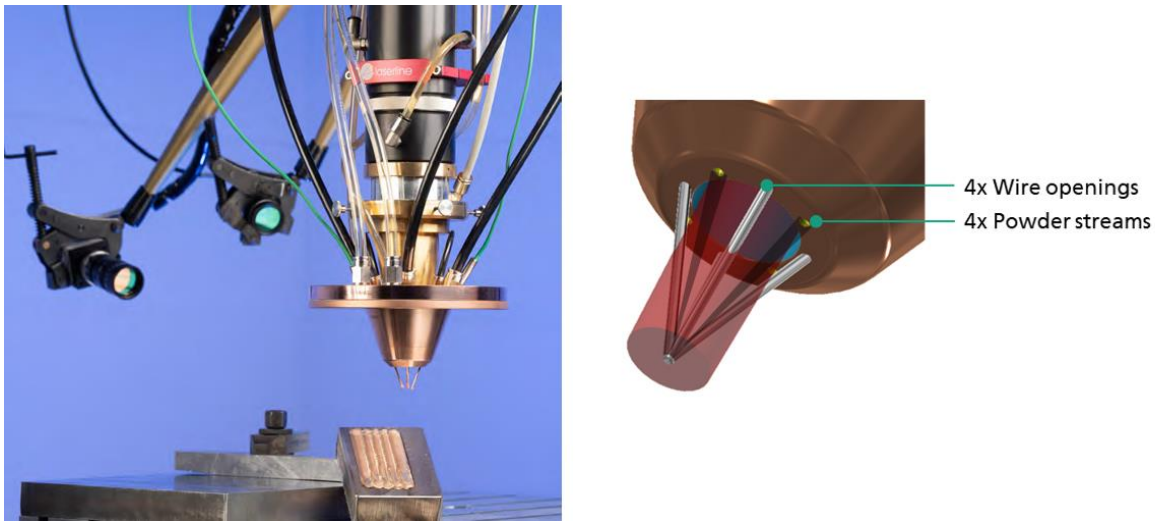

Figure 6 - Schematic representation of the COAXquattro nozzle **[4].**

2.4. Coating geometry

The produced clad meets predefined requirements. An important parameter that reflects the quality of the clad layer is the degree of dilution. This consists of the intermixing of the deposited coating and the substrate material: low dilution means a small amount of the substrate material is mixed with the coating **[39]**. The degree of dilution is given as the ratio of the surface or mass fractions of the base metal to the coating metal. Here, the clad consists mainly of the filler metal and a smaller, unwanted portion of substrate material brought by segregation **[28]**. Figure 7 shows the geometrical specifications of a clad, such as clad layer thickness (*Hc)*, width (*Wc*) and the areas of clad (*Ac*) and molten base materials (*Ab*), respectively.

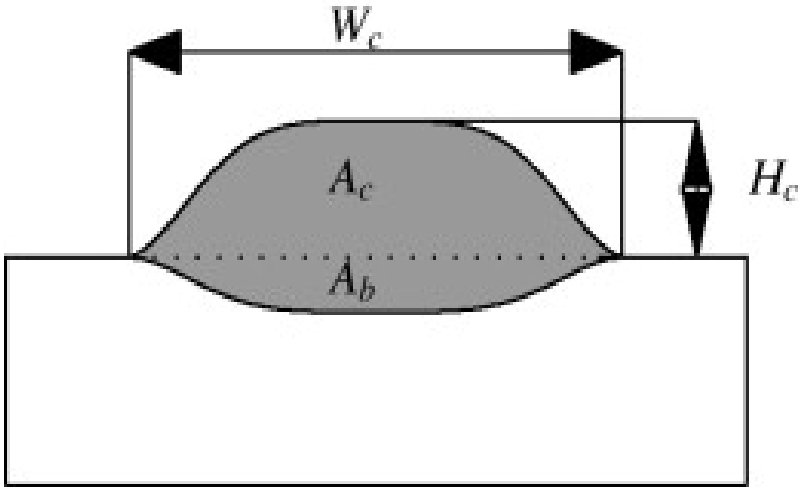

Figure 7 - Geometric data of a weld track and surface **[40].**

These parameters, resorting to equation (1.1), allow us to calculate the degree of dilution in the sample:

$$Dilution = Ab / (Ab + Ac) * 100 \qquad (1.1)$$

The goal is to obtain a coating with minimal dilution with the substrate material while maintaining metallurgical bonding between the different materials. If this ratio is zero, the risk of non-bonding is imminent. If dilution is too high, the deposited material may melt on the substrate and affect the chemical compositions, deteriorating not only the characteristics of the clad but also those of the base material **[41]**. Since this technology can produce coatings while using minimal heat inputs, the probability of occurrence of

distortion phenomena in the substrate reduces drastically, culminating in a smaller Heat Affected Zone (HAZ and dilution: the value for the last one is usually up to 3% **[39, 42]**.

The deposition quality depends on the formed angle between the filler material and the substrate (ß'). Figure 8 displays the three different tips that can happen during the process: left - the high degree of dilution is caused by a low feedstock deposition rate, and only part of the laser energy is absorbed by the filler leaving the rest to interact with the substrate; right - insufficient metallurgical bonding between the different materials, either caused by high cladding speed or low laser power; centre – the desired result, low dilution and considerable clad height **[43, 44]**.

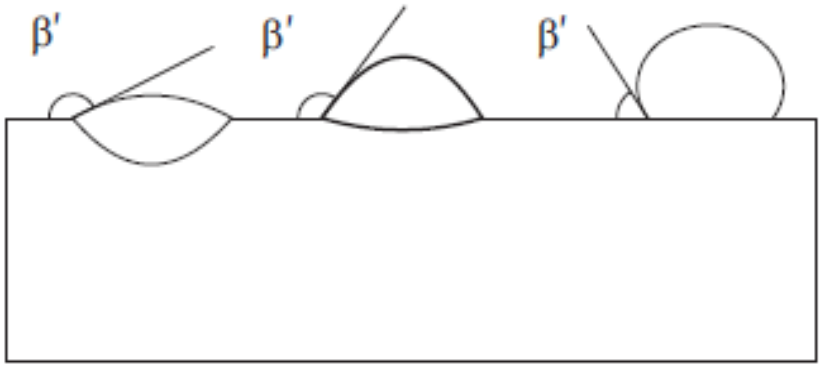

Figure 8 - Contact angle for different clads **[43].**

This concept gains importance when, instead of evaluating clad tracks individually, the analysis is made to a whole surface area of the coating, which leads to the obtention of the degree of overlapping within the tracks. This parameter, which is represented in Figure 9, quantifies the fraction of the track that overlaps with the other and is defined by equation 1.2:

$$OverlapRatio = Hc / Wc \qquad (1.2)$$

where Hc is the width of a single clad layer and Wc is its thickness **[45].**

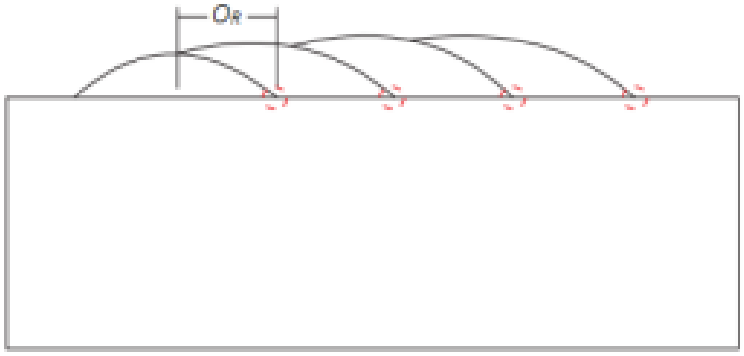

Figure 9 - Schematic view of overlapped layers **[45].**

While directly affecting the final thickness, which is expected to be homogeneous throughout the substrate, the overlap ratio is interconnected with dilution: low overlap means the dilution is too high, which translates into excessive mixing of the feedstock with substrate; if a high overlap value is used, dilution is heterogeneous, leading to the decrease of the functional properties of the coating **[46, 47]**.

2.5. Materials

Inconel 625, nickel-based superalloy, is a commonly used feedstock in laser cladding due to its high-temperature strength, excellent corrosion resistance and high ductility. Plus, this alloy is easily accessible in the market, being found in wire form with different diameters. These materials are commonly used in gas turbine ducting, furnace hardware, and components exposed to seawater **[49].** Combining the low dilution of the laser cladding with the excellent corrosion properties of the alloy, the uses were extended to the oil and gas industry. The corrosion resistance offered by the steels used in drilling equipment is limited as they suffer from localised corrosion in chloride-rich solutions. With that being said, the lifespan of offshore equipment is increased by laser coating the surface of the steels with Inconel 625 alloy **[50].** The microstructure of laser-cladded Inconel 625, which is similar to the microstructure depicted in Figure 10, is made of columnar dendrites that grow epitaxially from the substrate, following the direction of the thermal gradient.

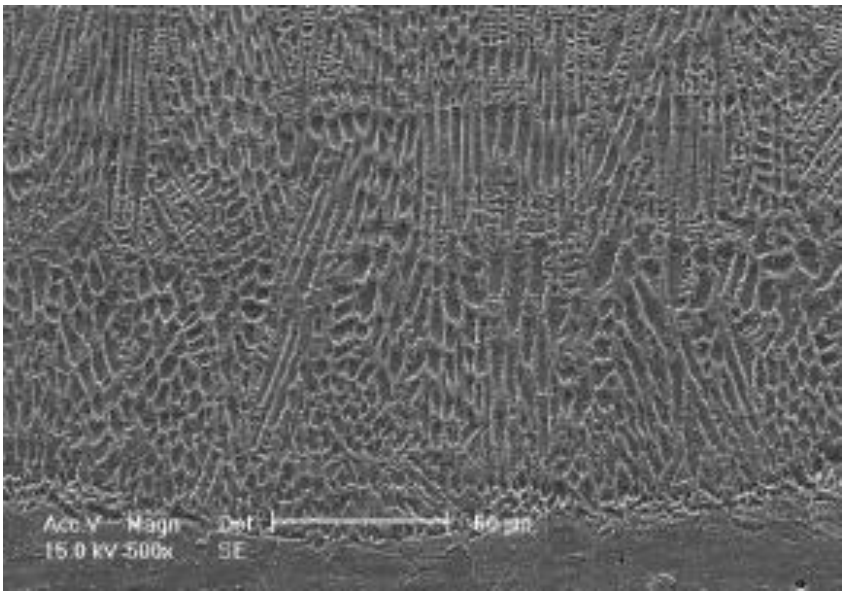

Figure 10 – Microstructure of Inconel 625 produced by DMD **[51].**

The superalloy is composed of the FCC austenitic (ϒ) matrix phase along with secondary phases that control the mechanical properties such as carbides (MC, $M_{23}C_6$, …), ϒ″ phase (Ni3Nb) and Laves phase **[52].** These coatings tend to present a less intermetallic phase with more strengthening elements remaining in solid solution as a consequence of the very high cooling rate of the process **[53].** It has been studied that NiCr coatings, deposited by laser cladding and plasma spraying, tend to degrade at temperatures above 700°C - 800°C, limiting their high-temperature application, as this causes a significant hardness and wear resistance decrease **[54]**. Increasing the coatings' thermal stability, under external and frictional heating, is an important research task. Often, Ni-based alloys are strengthened with tungsten carbides as these have highly stable hardness for temperatures up to 1000°C. The typically used carbides for this composite are titanium, chromium, and tungsten. The presence of WC is a protective shield against the penetration of erosive particles. Numerous studies were performed to correlate the characteristics of the coating with the loss of eroded material, with a few of them being displayed in Table 2. The volume fraction and the distribution of the WC particles in the matrix are the most important factors **[55, 56].**

Table 2 - Compilation of multiple laser cladding MMC coating procedures utilising tungsten carbides.

Method	Substrate	Hard particles	Matrix alloy	Mechanical properties	Ref.
Different content of WC	C45E, AISI 304, H13	WC	Metco 12C, METCO 16C, Ni60A	The improved hardness of the coatings	Ortiz *et al.* **[57]**, Tobar *et al.* **[58]**, Li *et al.* **[59]**
Different laser spot configurations	Q550 steel	WC	Ni60	Wide-band laser coatings displayed higher hardness and wear resistance than circular laser coating.	Ma *et al.* **[60]**
Preheated substrate	1Cr18Ni9Ti	WC	NiCrBSi	Coating was five times harder than the substrate; wear resistance increased with the increase of WC.	Guo *et al.* **[61]**
Laser induction hybrid cladding (LIHC) vs laser cladding (LC)	Medium carbon steel	WC	Ni-based alloy powder	Hardness of multi-track LIHC coating was lower than multi track LC coating.	Zhou *et al.* **[62]**

However, WC dissolution still presents an obstacle to achieving optimal performance of these coatings in wear and corrosive environments **[60]**. The abrasive wear performance of tungsten carbide/Ni base alloy MMC coatings has been researched. Huang *et al*. **[64]** revealed that the wear rate of the laser-clad layers increases with the decrease of retained WC particles in the coating. Also, Guo *et al*. **[61]** established that both wear and hardness of WC–Ni coatings increased due to carbon dissolution in the matrix.

The corrosion behaviour of these composite coatings has not been researched thoroughly. Liu *et al*. **[65]** studied the performance of laser-treated Inconel 625 and WC–Inconel 625 coatings: the MMC coatings showed lower corrosion resistance. This results from the microstructural modification after WC dissolution in the matrix. Lyanage *et al*. **[66]** established that this dissolution results in the precipitation of secondary carbides such as Fe_3W_3C, $Cr_{23}C_6$, Ni_2W_4C, Mo_3W_3C, etc. The contrast in electrochemical potentials between the carbides and the matrix results in complex galvanic couplings formation. Consequently, these coatings are more severely corroded. Therefore, it is of industrial and environmental relevance to study the influence of the carbide content in the coating wear and corrosion performance in order to maximise their durability and, consequently, optimise their cost-effectivity ratio.

Chapter 3

Experimental procedure

3.1. Process flow

The experimental procedure was performed in both Fraunhofer IWS Dresden, where the obtention of the laser cladding samples was conducted, and Faculdade de Engenharia do Porto (FEUP), *Departamento de Engenharia Metalúrgica e de Materiais*, where metallographic preparation and further mechanical properties testing occurred. The process flow is depicted in the flowchart presented in Figure 11. The samples were produced via laser cladding technology, resorting to the newest cladding nozzle created in Fraunhofer IWS, the previously mentioned COAXquattro, varying the main process parameters. Amongst the processed specimens, the most relevant ones to pursue further evaluation were chosen by building a Design of Experiments with Minitab. The input was the surface quality of the sample, analysed by visual inspection: the large batch was reduced to a group of 6 samples. These were then investigated in regard to microstructure, hardness, dilution and wear resistance. SEM/EDS was only used for comparison of the samples with different tungsten carbide percentages in the coating.

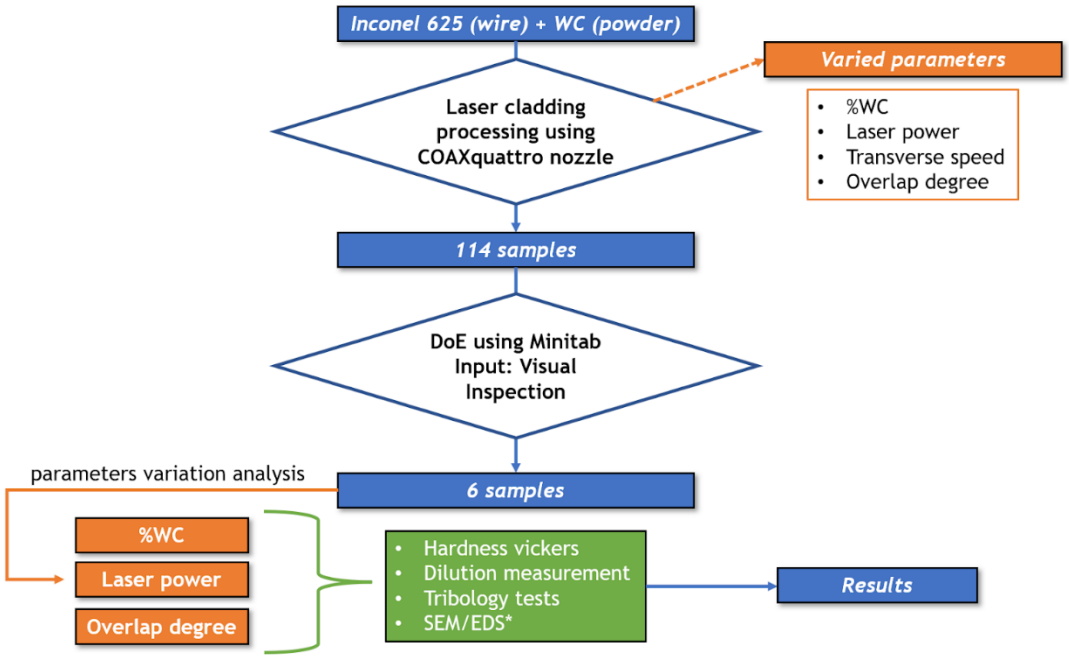

Figure 11 - Schematic representation of the process flow.

3.2. Materials

The composite was produced by *in-situ* mixing filler wire Inconel 625 alloy, Ø1.6 mm, with tungsten carbide spherical powder, particle size diameter 63-160 µm. Dinda *et al*. **[51]** investigated microhardness values of Inconel 625 processed via DMD, which values averaged 250 HV, without any post-processing. WC, the reinforcing material in the composite, displays an average hardness of 2600 HV **[67].**

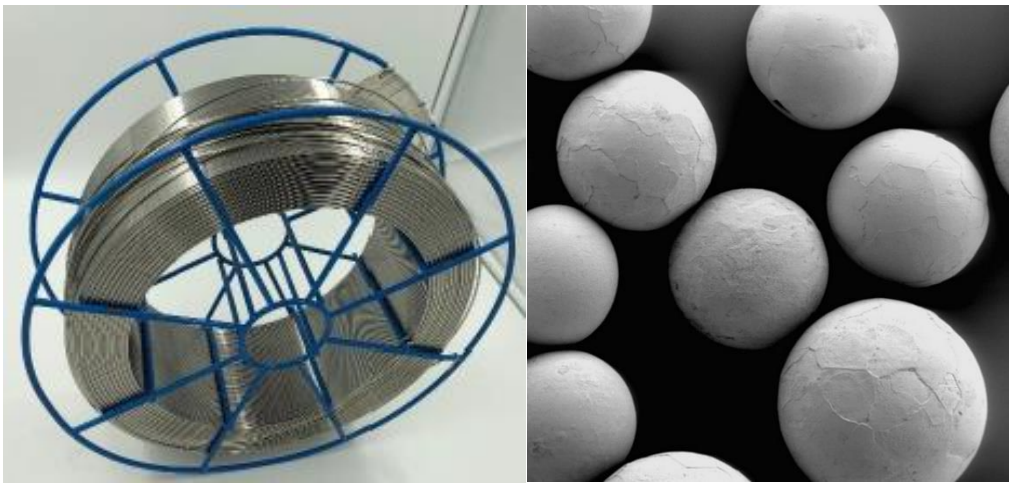

Figure 12 - a) Inconel 625 wire representation; b) SEM image of the spherical WC powder **[67].**

Table 3 - Feedstock chemical composition **[67,68].**

Material	Ni	Cr	Mo	Fe	Nb+Ta	Co	Mn	Al	WC
Inconel 625 wire	58-71%	21-23%	8-10%	5%	3.2-3.8%	1% max	0.5% max	0.4% max	-
Tungsten carbide powder	-	-	-	-	-	-	-	-	100%

The substrates are made of mild steel S235, which was available at the institute in dimensions of 80 x 40 x 10 mm. This alloy is standardised according to DIN 10025-2 as hot-rolled and unalloyed structural steel with good weldability and toughness. The average hardness for this material is around 120HV **[69].**

3.3. Laser Cladding System

3.3.1 Testing Plant

Figure 13 shows the setup of the experimental plant used for this works' investigations. For handling and moving the processing head, devices such as robots or CNC processing centres are required. In this case, the cladding head is coupled to a 6-axis KUKA KR30 robot.

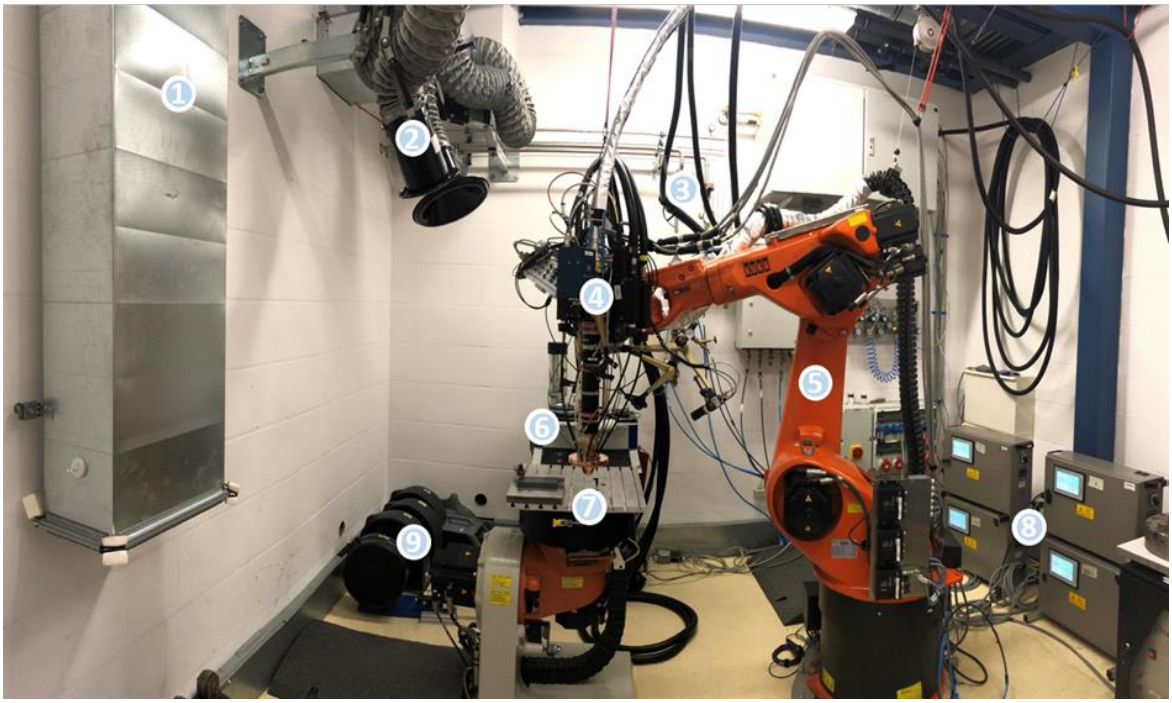

Figure 13 - Testing plant

1. Fresh air supply
2. Suction
3. Cooling
4. Processing head
5. Kuka KR30 robot
6. Powder conveyor
7. Working table
8. Wire control units (4x)
9. Additional feed with wire rolls (4x)

The testing plant, presented in Figure 13, integrates a fresh air supply (1), which is constantly renovating the laboratory's air, and two extractors (2), that remove the gases generated during the cladding process. In addition, the facility includes a cooling system (3) for the optics and the cladding head. Furthermore, the robot (5) with the respectively attached processing head (4) is also within the facility, as well as the working table (7),

which serves as a support for workpieces and clamping devices. The rear area of the laboratory is where the powder conveyor (6), the four wire controlling units (8) and the four additional feeders, each with a wire roll (9), are located. The powder used as feedstock is held in a pot, being then led by means of a conveyor through powder hoses to the processing head. Likewise, the additional feeders with the wire rolls are connected to the head via roll liners and their controlling units.

For operating and programming the industrial robot, the KCP (KUKA Control Panel) is utilised, which has all the operator control and display functions required **[70].** This teach pendant device, which is represented in Figure 14, is given the specific movement instructions based on the coordinates of the area to be coated within the substrate and is also the interface used to change the testing parameters within the running program.

Figure 14 - KCP (KUKA Control Panel), teach pendant device.

3.3.2 Laser and Optics

The diode laser device LDF 20000-200, from the company Laserline GmbH, was used to conduct the cladding. The 20 kW used laser is located outside the experimental laboratory and is connected to the processing head via a fibre to the optics, operating in a wavelength range of 940-1060 nm. The 2-inch optic built into the head is one of the Laserline OTS 2 series of collimating type Laserline 81 mm, with a fibre diameter of 2000 µm, a focusing focal length of 500 mm, and a spot diameter of 12.3 mm **[71].** This device can be configured using an integrated control panel, which is used for error detection and real-time diagnostics. The laser device itself is monitored via remote software, using a machine control station.

3.3.3 Processing Head

Figure 15 shows the processing head. The laser fibre is connected to the processing head by the optics (3), that is mounted on the mounting plate (4). This last one is coupled to the robot (5) using a flange. Also attached to the plate, using a hydraulic articulated arm, is the processing camera (6), which records the cladding process; and the laser incident light (7), that shines on the workpiece (9) at a specific wavelength, so that the camera records a video with the correct filter. Furthermore, one can see the wire conveyor units (2), which convey the wire through the roll liners (1) from the additional feeders with wire rolls to the cladding head (8).

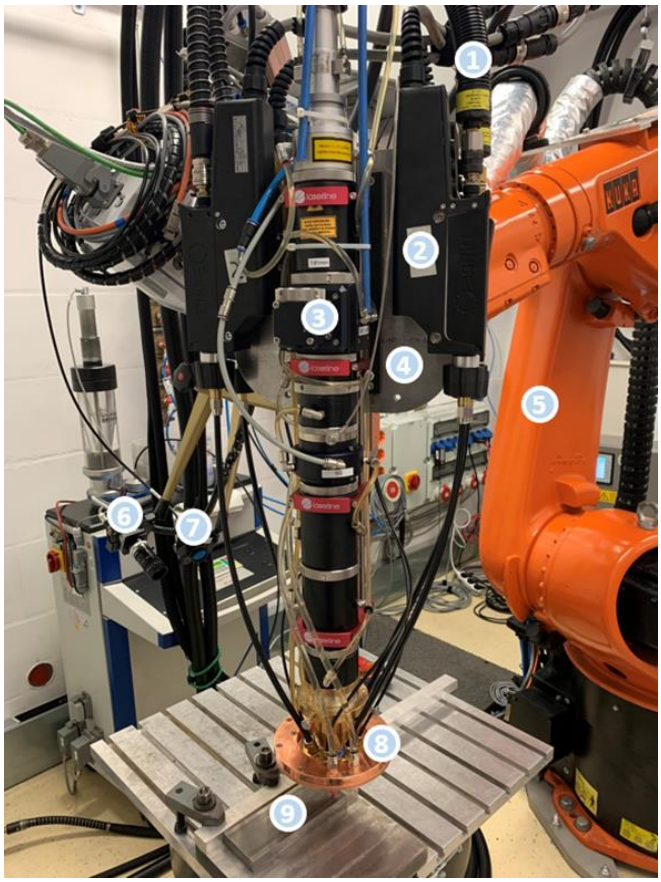

Figure 15 - Testing setup

1. Roll liner
2. Wire feeding units 4x
3. Optics
4. Mounting plate
5. Kuka KR30 robot
6. Processing camera
7. Laser incident light
8. Cladding head
9. Workpiece

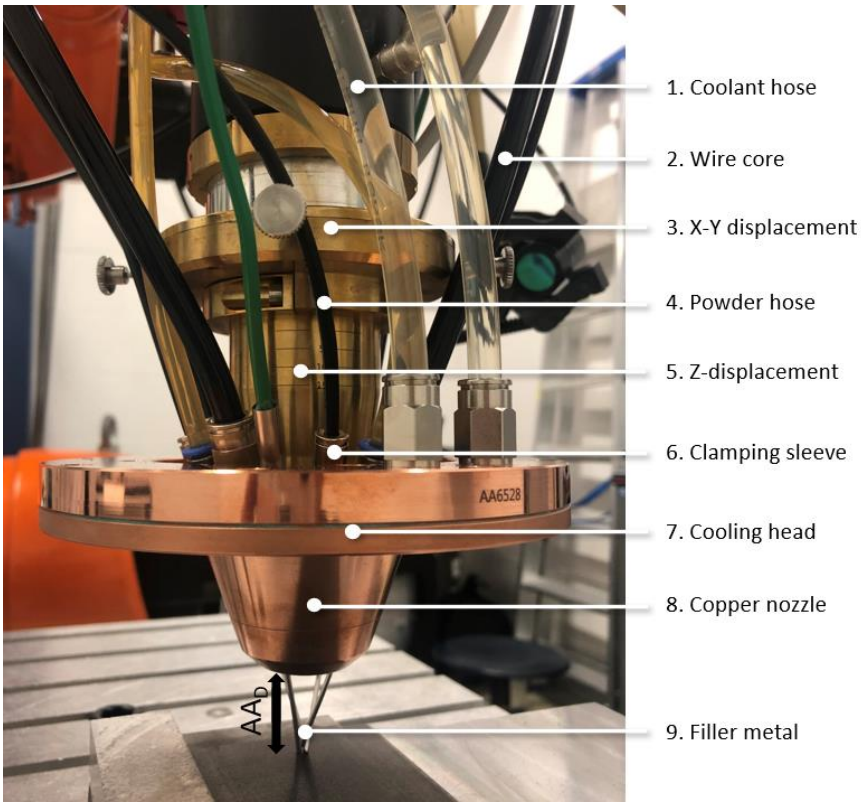

Figure 16 - Cladding head, see also position 8 in figure 15.

The cladding head, illustrated in Figure 16, is mainly composed of a cooling head (7), a copper nozzle (8) and X-Y, Z displacements. These last ones are responsible for fine adjustments of the head: Z offset for more precise focal length adjustment and the X-Y offset for centering the laser to the nozzle. Furthermore, coolant hoses (1), wire cores (2) and powder hoses (4) are connected to the nozzle with clamping sleeves (6). In addition to normal cooling, the cooling ring cools the copper nozzle during the cladding process. The wire cores guide the wire from the feeding units to the copper nozzle, and emerge from the nozzle end as filler metal (9). Similarly, the powder is conveyed from the powder distributor through the powder hoses to the nozzle.

3.3.4 Cladding Flow

The movement during the cladding process can be divided in three different sections. First, the nozzle is pre-positioned in the workpiece. At the beginning of the coating path both the powder, wire and laser are switched on and adjusted by delays, so that the laser hits the workpiece surface, a few milliseconds before the feedstock, to create a melting pool. As soon as the filler material enters the pool, the cladding process begins and the track is created. At the end of the clad, the feedstock is retracted before the laser is switched off. The movement to a safety distance completes the motion sequence, so that in the future, the head can be safely removed from the cladding area.

3.4. Design of Experiments

Leingruber *et al*. **[28]** experimented multiple testing parameters to utilise while processing Inconel 625 wire with COAXquattro. The mixing of Inconel 625 wire and WC powder cladding was then conducted by Doan *et al*. **[72],** based on knowledge obtained from laser wire and powder cladding individually. Suitable answers were attained by varying, systematically, the primary parameters: Laser power and transverse speed. In addition to the above parameters, other elements such as the powder percentage in the matrix and overlap ratio were also varied. After each test, the clads were analysed by means of visual inspection and video recordings, providing information about any inaccuracies, which were later one counteracted in subsequent tests by targeted parameter changes. The same concept was implemented during this work. The starting point was performed using the best parameters acquired by Doan *et al*. **[72]**, represented in Table 4, with backgrounds colored in grey. Whenever alterations were done, only one parameter was changed at a time.

Table 4 - Representation of the parameter changes throughout the study.

Parameters	Variation
Laser power (W)	9900, 10450, 11000, 11550, 12100
Transverse speed (mm/min)	1120, 1260, 1400, 1540, 1680
WC (%)	40, 50, 60, 70
Overlap ratio (%)	20, 30, 40

A design of experiments was built with the parameters shown in Tab.4 utilising *Minitab*, a leading software for data analysis. The overall goal for the utilisation of this software was to understand the interaction between these parameters, organise the conditions used in the multiple conducted experiments and, most importantly, have a data analysis tool to help choose the best samples to be studied after being obtained. For that matter, in order for the software to be able to choose the best amongst the multiple combinations of parameters, the chosen input was the cladding surface quality.

3.5. Characterization

3.5.1 Metallographic Preparation

The flowchart displayed in Figure 17 sums up the metallographic preparation of the samples to be used in each of the characterization methods approached in this study. Samples for dilution measurements, hardness tests and SEM/EDS analysis, followed the same route (except for the fact that the last method did not require previous etching). Samples to be tested regarding tribology followed a different path.

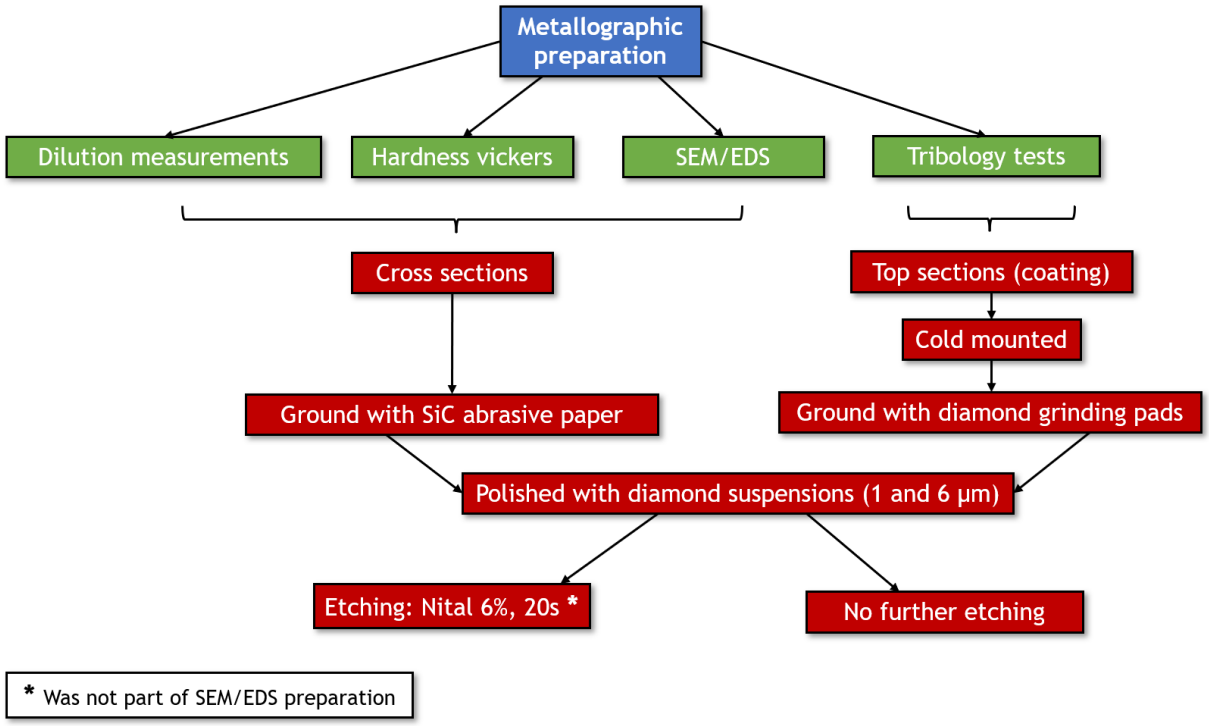

Figure 17 - Schematic representation of the conducted metallographic preparation.

3.5.2 Dilution Measurements

The degree of dilution was calculated for each sample, resorting to equation (1.1). The software ImageJ was used, as it can determine area value statistics of user-defined selections. The real values used in equation (1.1) were the total sum of the areas measured in the multiple beads. This calculation was conducted for all samples.

3.5.3 Hardness Testing

Microhardness Vickers testing was conducted according to the standard ISO 6507-1:2018 **[73]**. For each sample, three hardness profiles were obtained (one for each of the clads) using a diamond indenter with a load of 2.942 N, at room temperature. The indentations are homogeneously distanced along the profile, both in coating and substrate, as it is shown in Figure 18. The starting place for the indentation profiles was chosen randomly near the centre of each clad, so that the number of hardness values within the same coating clad was maximised.

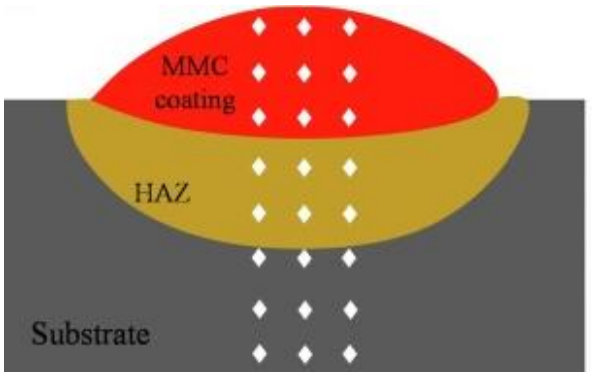

Figure 18 - Schematic representation of the hardness tests, adapted from **[74].**

3.5.4 SEM/EDS Analysis

In order to understand the influence of the increase of tungsten carbide powder in the matrix of the composite, both in terms of microstructure and carbides distribution, some samples were analysed with aid of a scanning electron microscope (SEM), FEI QUANTA 400 FEG ESEM. Energy dispersive X-ray spectroscopy (EDS) tool was used for chemical analysis of the samples' cross-sections.

3.5.5 Tribology Tests

The wear resistance of the composite was further assessed by the utilisation of a tribometer. The machine functions with a pin-on-plate concept, in which a specific load is applied on the pin, containing an alumina sphere with a diameter of 4 mm, that establishes contact with the sample surface, Figure 19. A relative sliding motion is then administered between the pin and the surface through a reciprocation motion, during a pre-selected duration of the test. The samples were placed in the sample holder, serving the purpose of plate during the tests. As this test aims to evaluate wear resistance of in-service components, the tested area is now the top part of the coating. These experiments were conducted with a load of, approximately, 5 N, while the plate was moving with a frequency of 1 Hz, on a 6mm track length. The selected duration was 30 minutes. The worn area was calculated with the software ImageJ, which was previously used in the dilution measurements.

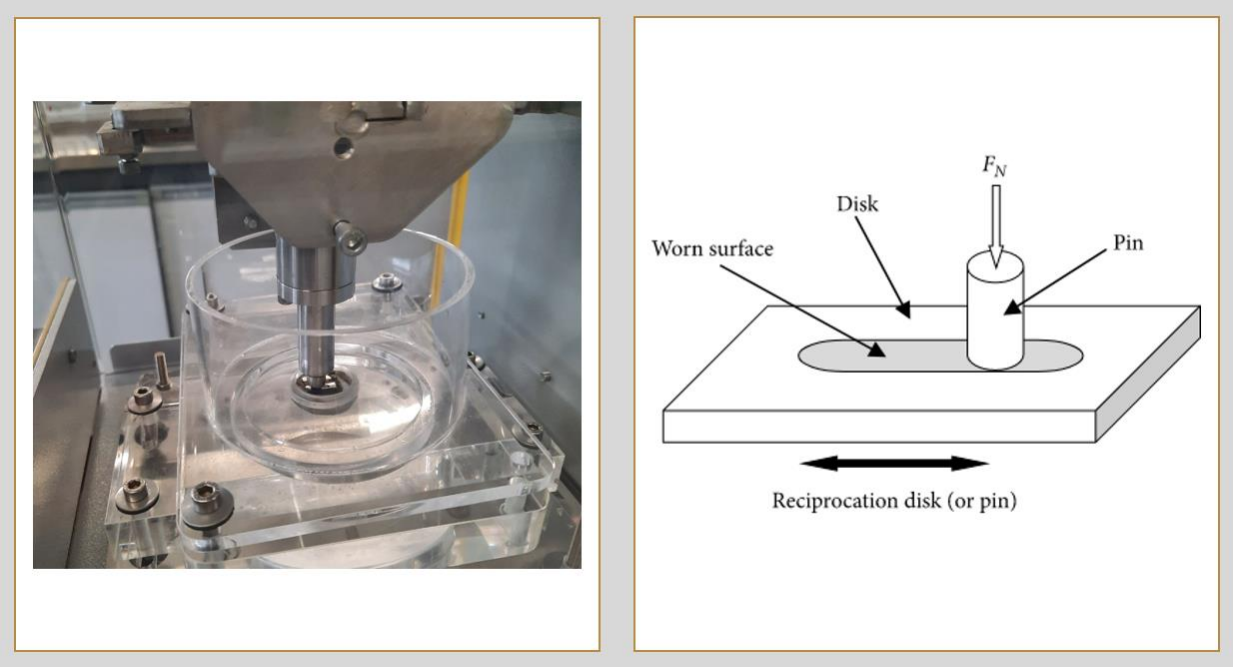

Figure 19 - Schematic representation of the pin-on-plate tests, adapted from **[75].**

Chapter 4

Results and Discussion

4.1. Design of Experiments

The design of experiments was built utilising the surface quality as the input. It was predefined that all samples would be ranked from a 0 to 4 scale regarding the quality of the cladding (0-Very bad; 1-Bad; 2-Average; 3-Good; 4- Very good). Figure 20 aims to represent the difference in surface quality for each of the levels mentioned. Level 0 - the picture suggests that there was not enough laser power to melt the feedstock and achieve metallurgical bonding with the substrate; Level 1 - same thing happens when compared to 0, only to a different degree: the lack of laser power is not so prominent; Level 2 - the dilution seems to have been reduced drastically but, there is a considerable irregularity in the borders of the beads (high transverse speed), existence of cracks (high tungsten carbide content) and solidification of the bead under blue coloration (associated with high laser power); Level 3 - the irregularity of the borders was fixed and the depth of the cracks decreased, there is still some blue coloration, suggesting too much laser power; Level 4 - the pre-described problems seem to have been corrected.

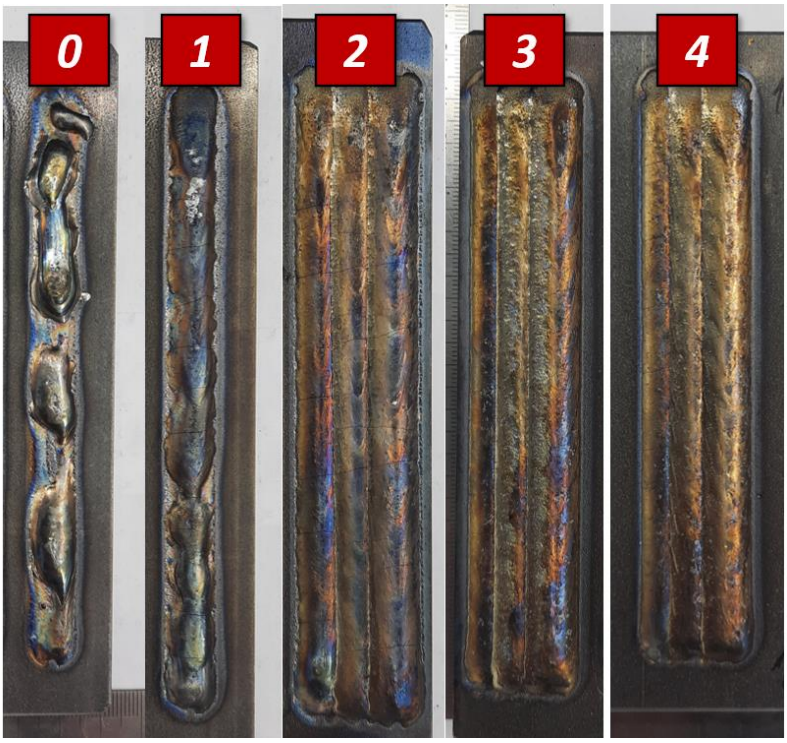

Figure 20 - Representation of the different surface quality levels used for DoE construction.

The created factorial design was further analysed to determine which specific conditions played a bigger role regarding surface quality of the clad. With the following graphs shown in Table 5, it was possible to conclude that, to enhance quality: 70% WC should be forgotten, 9900 and 11550 W laser power did not help achieving the best quality and, most significantly, transverse speed should be fixed at 1400 mm/min.

Table 5 - Main effects plot for surface clad quality

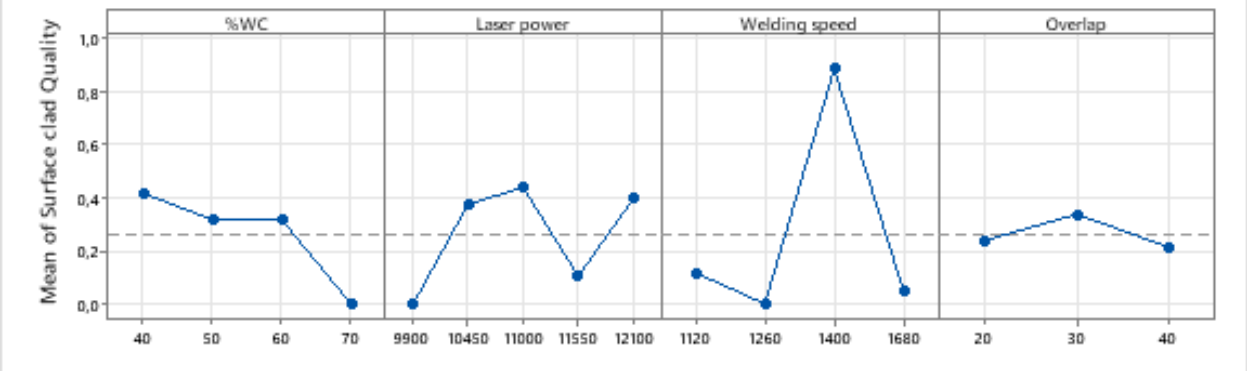

Lastly, Minitab's 'Response Optimizer' tool was used. This allowed us to identify the combination of input variable settings that optimise a response, in this case the surface quality displayed by the samples, by calculating the chosen optimal solutions and drawing an optimization plot. Table 6 presents the ordered results for the optimization plotted by the software: from the nine displayed solutions, numbers 1 to 5, and 7 (with orange and blue backgrounds) were chosen for further study and evaluation.

Table 6 - Plotted solutions given by Response Optimizer.

Solution (+ sample number)	%WC	Laser power	Transverse speed	Overlap	Surface Quality Fit	Composite Desirability
1 (70)	50	12100	1400	30	4.00000	1.00000
2 (80)	40	10450	1400	40	4.00000	1.00000
3 (72)	40	10450	1400	30	3.99167	0.99792
4 (76)	40	10450	1400	20	3.99167	0.99792
5 (74)	40	12100	1400	30	3.80417	0.95104
6	50	11000	1400	20	3.26667	0.81667
7 (10)	60	12100	1400	30	3.02083	0.75521
8	40	11000	1400	20	2.86667	0.71667
9	50	12100	1400	20	2.70417	0.67604

4.2. Dilution Measurements

As it was previously mentioned, the degree of dilution is an important parameter that reflects the quality of the clad layer **[39]**. The goal is to obtain a coating with minimal dilution, while maintaining metallurgical bonding between the different materials **[41]**. Dilution depends directly on the chosen processing parameters during laser cladding: laser power, tungsten carbide percentage, transverse speed and overlap ratio. The increase in laser power implies the increase of energy input, which enhances the probability of distortion phenomena in the substrate, culminating in larger HAZ and dilution **[42].** Amongst the materials that are part of the composite, Inconel 625 is the one with the highest thermal conductivity. With that being said, the increase in tungsten carbide content in the matrix reduces the thermal conductivity of the composite, which diminishes the possibility for causing dilution. By increasing the speed in the cladding process, the energy input per unit of time is reduced, decreasing dilution. Lastly, low overlap translates into excessive mixing of the feedstock with the substrate **[46]**. Figure 21 aims to represent the selection of areas to be measured as *Ab* and *Ac*, displaying only the cladding zone of the first bead. Table 7 shows the degree of dilution obtained for each sample after having been processed via laser cladding technology.

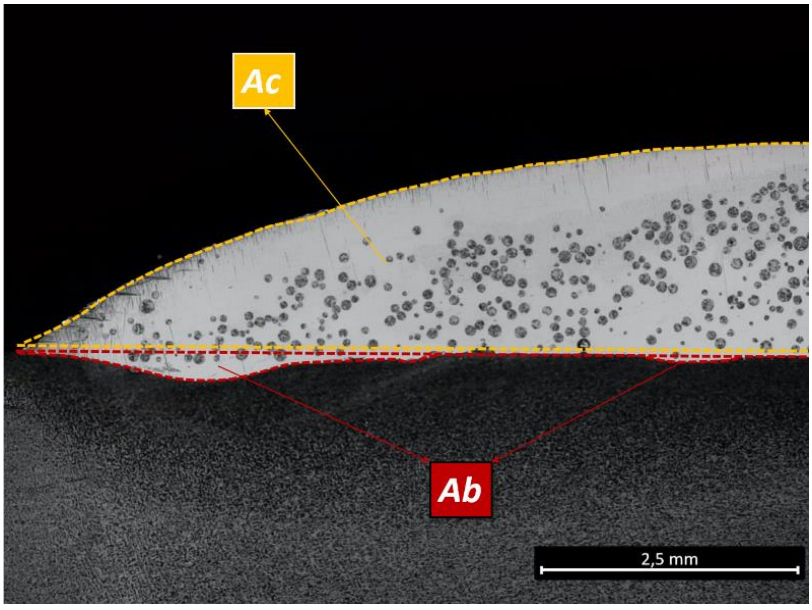

Figure 21 - Schematic representation of the measured areas for dilution calculation.

Table 7 - Dilutions summary for the different samples.

Processing parameters					Dilution calculation		
Samples	%WC	Laser power W	Transverse speed mm/min.	Overlap ratio (%)	*Ab* (mm^2)	*Ac* (mm^2)	Dilution (%)
1 (70)	50	12100	1400	30	1.677	48.611	3.33
2 (80)	40	10450	1400	40	0.446	36.760	1.20
3 (72)	40	10450	1400	30	0.750	34.772	2.11
4 (76)	40	10450	1400	20	0.820	37.054	2.16
5 (74)	40	12100	1400	30	2.001	50.980	3.78
7 (10)	60	12100	1400	30	1.042	40.002	2.54

While assessing the data available in Table 7, it is possible to visualise that the group of samples 80, 72 and 76, the ones produced with the same laser power and tungsten carbide percentage (10450 W and 40%WC), showed the lower degree of dilution (1.20, 2.11, 2.16, respectively); samples 70, 74 and 10, the group both laser power and degree of overlap in common (12100 W and 30%), displayed the higher measured values (3.33, 3.78, 2.54, respectively). As the decrease in tungsten carbide content in the matrix increases the thermal conductivity of the composite and the possibility for causing dilution, the fact that samples 80, 72 and 76 (all with 40%WC) exhibited lower dilution, proves that laser power is the most important parameter in the existence of dilution. By establishing a comparison between the measured values for that same group of samples, it is possible to study the role played by the overlap ratio in the dilution of the specimen. Their results show that dilution decreased with the increment in overlap. While looking at obtained results for samples 70, 74 and 10, it is also visible that, not only a higher laser power

produced the worst samples regarding dilution, but also that the increase in tungsten carbide content implied a reduction of measured dilution. Overall, the less mixing of the coating with the substrate was achieved with lower laser power and higher degree of overlap. Even though some samples presented a quite better result, the measurements did not exceed largely the value of 3%, as quoted in the literature **[42].**

4.3. Hardness Testing

Figure 22 intends to represent the different hardness measured areas in the specimen, showing the cross-section of one of the laser cladding processed samples. Figure 23 shows some captured images of the indentations' neighbour areas, both in the coating (left) and substrate (right). Whilst analysing the left image, it is possible to identify the large spheres of tungsten carbide, distributed throughout the Ni-matrix (white background). However, these are not the only identifiable phases: the laser processing induced partial dissolution of the WC, which resulted in the formation of secondary carbides (grey dendrites over the matrix). These will be assessed further in this work, via chemical analysis. The image on the right represents the microstructure of the S235 mild steel, used as substrate material. As it was expected, the high inputted laser energy caused the formation of a martensitic structure, typical for quenched and tempered heat treatments.

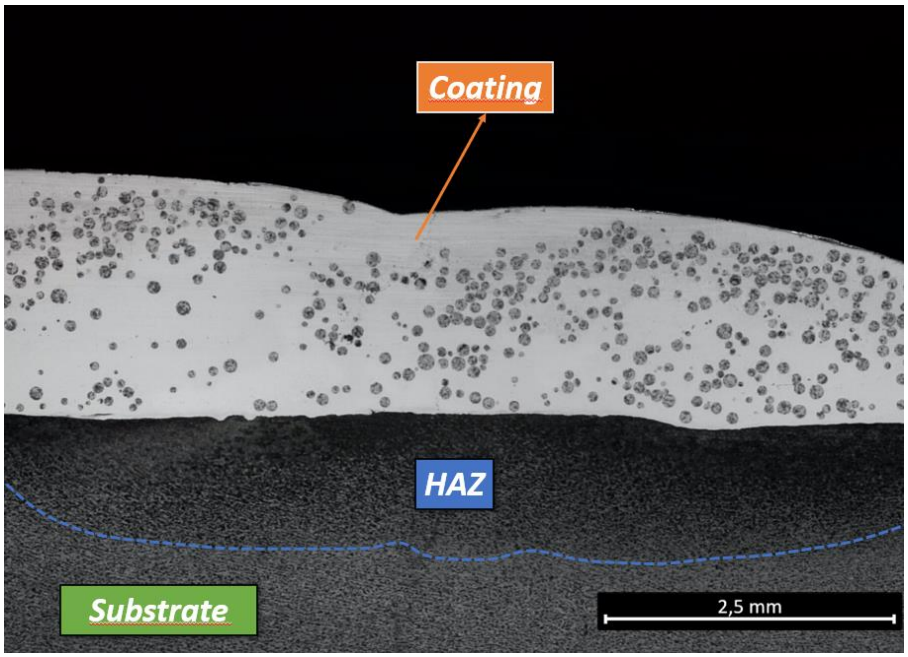

Figure 22 - Schematic representation of the samples' cross-section.

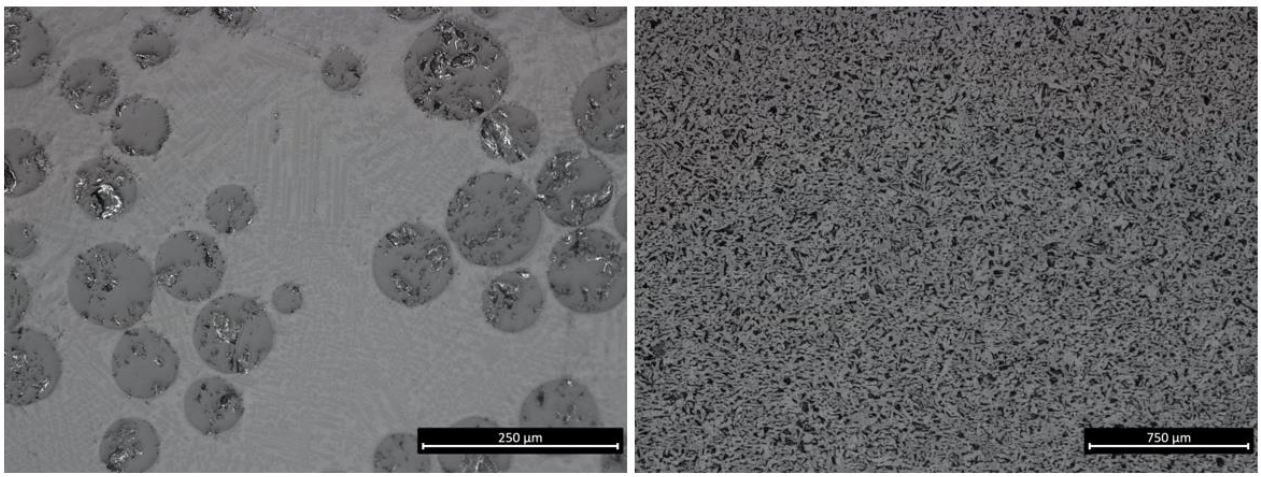

Figure 23 - Microstructural analysis of the samples' coating and substrate.

Vickers microhardness results, presented in Table 8, consist of an average of the measurements conducted in each one of the three clads per sample, Figure 24. In every single case, the composite displayed an increase in hardness when compared to measurements made to pure Inconel 625 processed by LC. This, theoretically, results from, not only from the addition of tungsten carbide powder (that has roughly 2600 HV), but also because it partially dissolves due to the extreme high energy input. This leads to the formation of hard phases such as W_2C, M_6C and topologically close-packed (TCP) phases **[76, 77].**

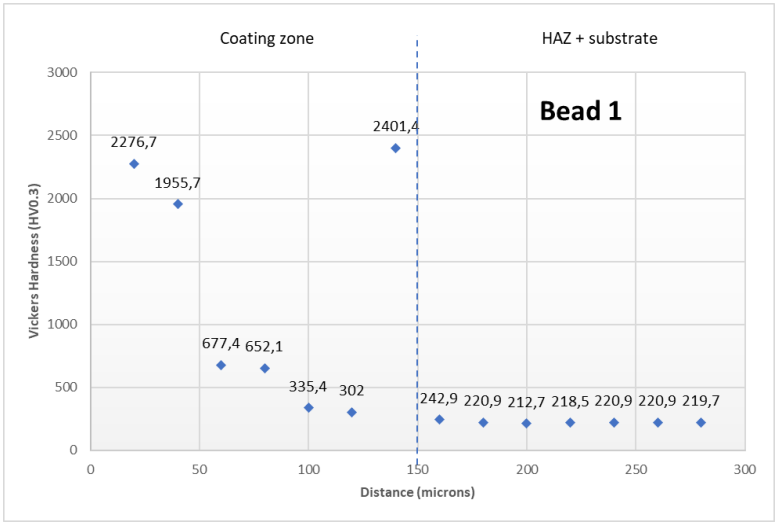

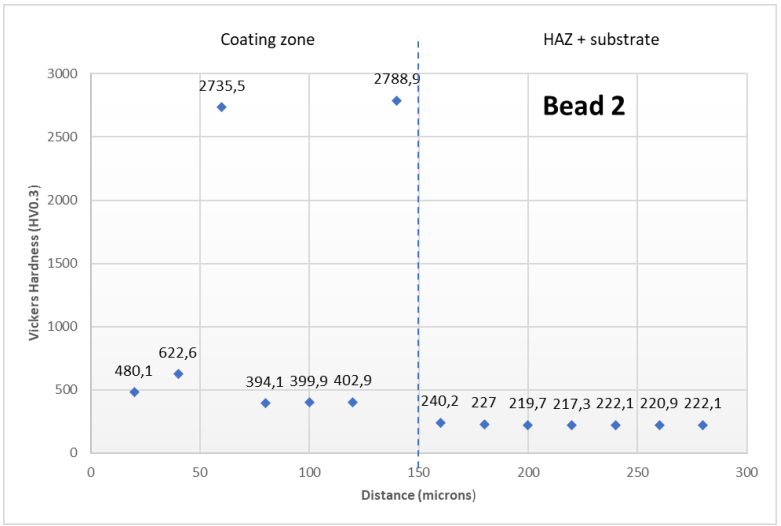

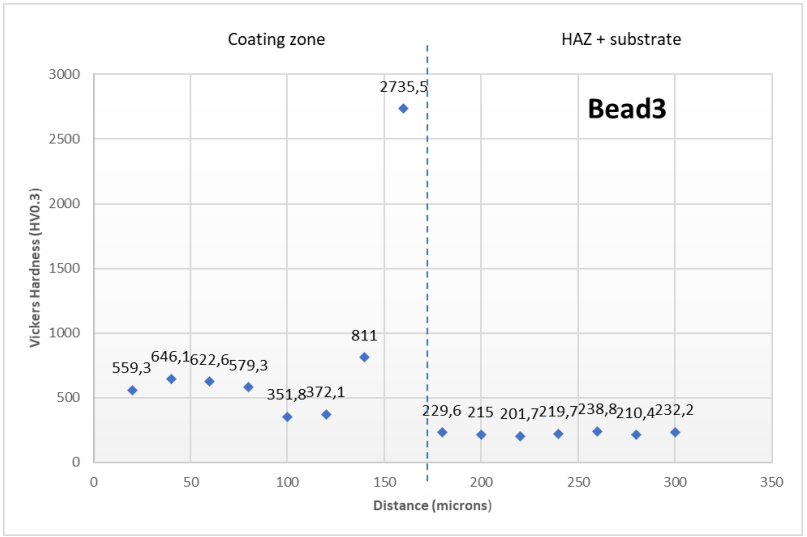

Figure 24 - Representation of the hardness values along the profiles for a sample.

Table 8 - Hardness property summary for the different chosen samples.

	Processing parameters				Hardness value (HV0.3)	
Samples	%WC	Laser power W	Transverse speed mm/min.	Overlap ratio (%)	Coating	HAZ + substrate
1 (70)	50	12100	1400	30	1114	223
2 (80)	40	10450	1400	40	914	215
3 (72)	40	10450	1400	30	984	217
4 (76)	40	10450	1400	20	1060	222
5 (74)	40	12100	1400	30	1053	221
7 (10)	60	12100	1400	30	1122	222

When directly establishing a comparison between samples 70, 74, and 10, it is visible the hardness improvement in the coating area, as the percentage of tungsten carbide in the composite goes from 40 to 50, and then to 60%, with the last one presenting the highest average measured value of 1122 HV. From samples 80, 72, and 76, as the rest of the parameters were maintained, it is possible to assess the result of the overlap ratio's variation: by increasing it, the average hardness value of the samples' coatings decreased from 1060 HV (20% overlap) to 914 HV (40% overlap). This fact is corroborated by the bibliography **[78]**. By looking at these same samples' hardness values in the HAZ, even though the difference is slight, the increase in overlap ratio caused a decrease in the measured values. This fact can be explained by the reduction of the contact area between the laser beam and the substrate and the distribution of the thermal input by a larger deposited material volume **[45]**. Plus, the increase of the overlap promotes a decrease in hardness by reducing the solidification speed. Lastly, the influence of laser power can be

approached by comparing samples 72 and 74: the increase in energy per unit time of laser (10450 to 12100 W) resulted in a direct escalation of the measured hardness values (984 to 1053 HV). The higher energy input leads to more tungsten carbide dissolution, which promotes the formation of the before mentioned hard phases in the microstructure, thus explaining the hardness rise. The hardness increase for the substrate results both from the material intermixing with the coating (even if slight), and from the resultant heat of the processing, which acted as a heat treatment for the specimens.

4.4. SEM/EDS Analysis

The microstructure of laser cladded Inconel 625 coatings is made of columnar dendrites that grow epitaxially from the substrate, following the direction of the thermal gradient **[51].** However, by adding tungsten carbide into the matrix, the growth of the grains changes its direction. They start growing perpendicularly to the centre of the WC spheres, due to the very high cooling rate, gradually transforming from columnar to equiaxed grains **[79].** The illations made in this chapter regarding phase identification in the composite were supported by EDS and XRD tests conducted in the literature **[51, 63, 77, 79].** The following pictures depict the morphology of the different samples at various magnifications. First off, it is possible to acknowledge that the tungsten carbide distribution gets less homogeneous as the powder content in the composite reduces. In Figure 25A, which represents sample 10 (the one with the highest ceramic content), not only the density of the spheres in the coating is higher, but also WC distribution is the most homogeneous. This same content and distribution fade away as the powder percentage reduces, Figure 25C. Also, it is visible that the upper part of the coating presents less WC quantity. Some porosity may be visible in all inspected samples.

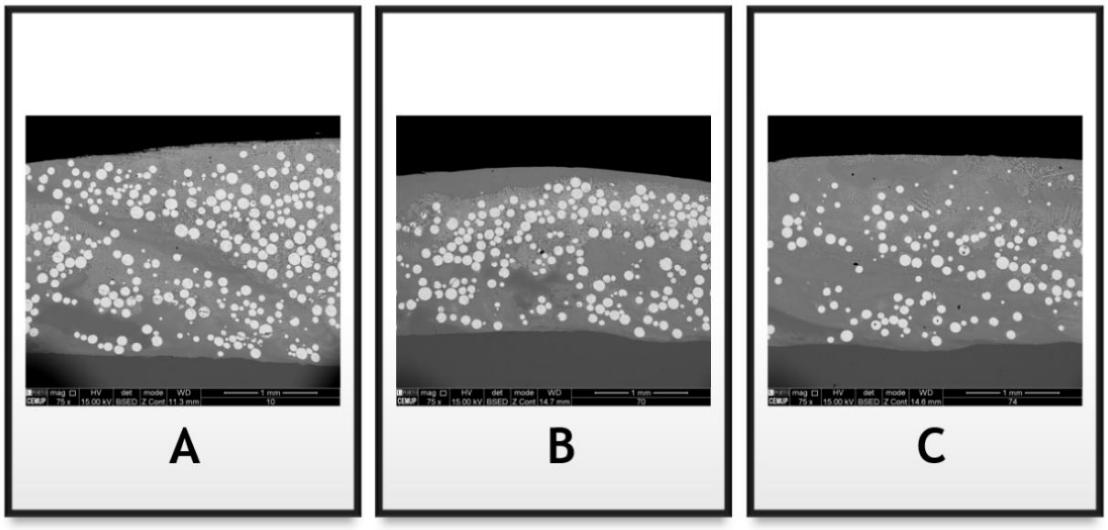

Figure 25 - SEM images of the different samples' microstructure. A - 60% WC; B - 50% WC; C - 40% WC.

Figure 26 includes several taken images of sample 10, in which tungsten carbide powder content was the highest of the batch (60%). Chemical composition of zones 1 to 4 was analysed with aid of EDS. The results are depicted in Table 9.

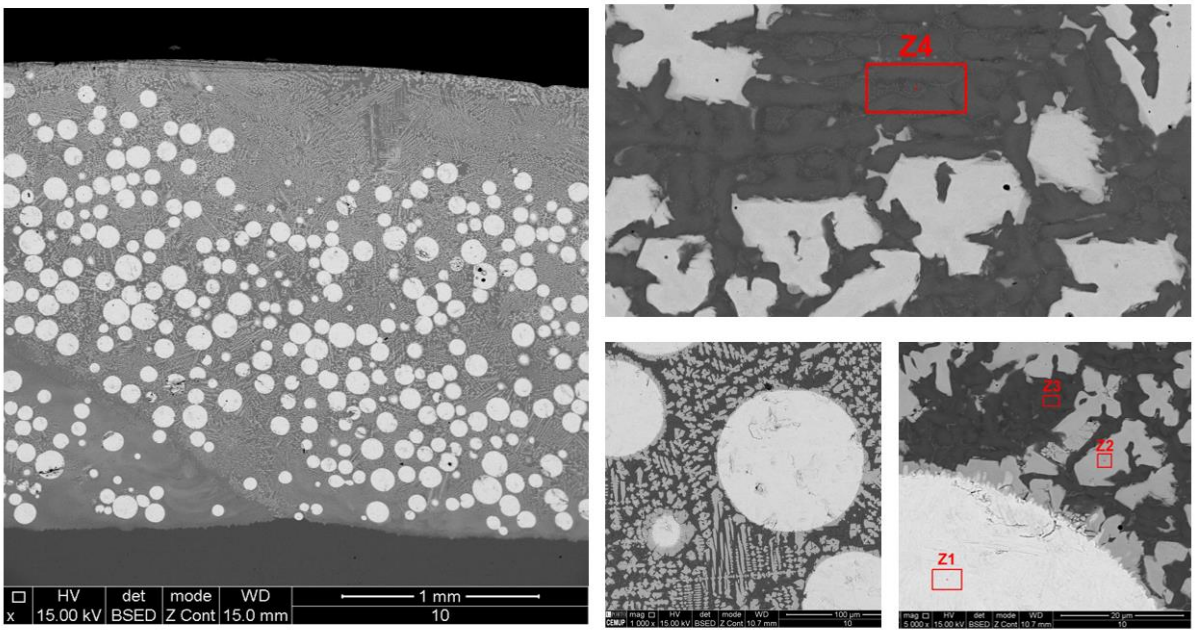

Figure 26 - SEM images of sample 10, alongside EDS's analysis zones.

Table 9 - Chemical analysis of phases in coating/wt-%, sample 10.

Symbol	W	C	Cr	Fe	Ni	Nb	Mo	Phase
Z1	98.62	1.38	-	-	-	-	-	WC
Z2	59.56	1.13	9.69	0.97	19.48	-	9.15	W_2C
Z3	63.70	1.02	7.91	1.4	17.74	-	8.24	M_6C
Z4	14.38	1.01	17.88	4.02	57.71	-	5.01	γ-Ni matrix

The chemical analysis of zone Z1, which consists of part of a tungsten carbide sphere, naturally shows the presence of W (in majority) and C. The phase that is analysed as zone Z2, which is a highly present eutectic phase in most of the microstructure shown in Figure 26, consists of W_2C and is a natural consequence of the microstructural modification after WC dissolution in the matrix, because of the high imposed temperatures. During the deposition process, tungsten diffused in the γ-Ni matrix, while carbon stayed in the intergranular region, leading to the precipitation of secondary carbides. The chemical analysis of zone z4 shows a majority of Ni and Cr, with some relevant decrease of tungsten content. With that being said, this zone can be taken to be the γ matrix. Lastly, zone Z3 reveals composition similar to Z2, and may very well be associated with being intergranular precipitation of M_6C. This secondary carbide, which is suggested by Lyanage *et al*. **[63]** to be either Fe_3W_3C or Mo_3W_3C, results from element segregation, such as Mo and C, after being exposed to the high temperatures of the laser cladding process. In general, main alloying elements Ni and Cr were found in the matrix, while Fe and W were spread throughout the sample. This proves tungsten diffusion inside the matrix, as a consequence of the imposed high temperature.

Figure 27 comprises acquired images of sample 70, in which tungsten carbide powder content in the matrix of the composite is 50%. Chemical composition of zones 1 to 4 was analysed with aid of EDS. The results are shown in Table 10.

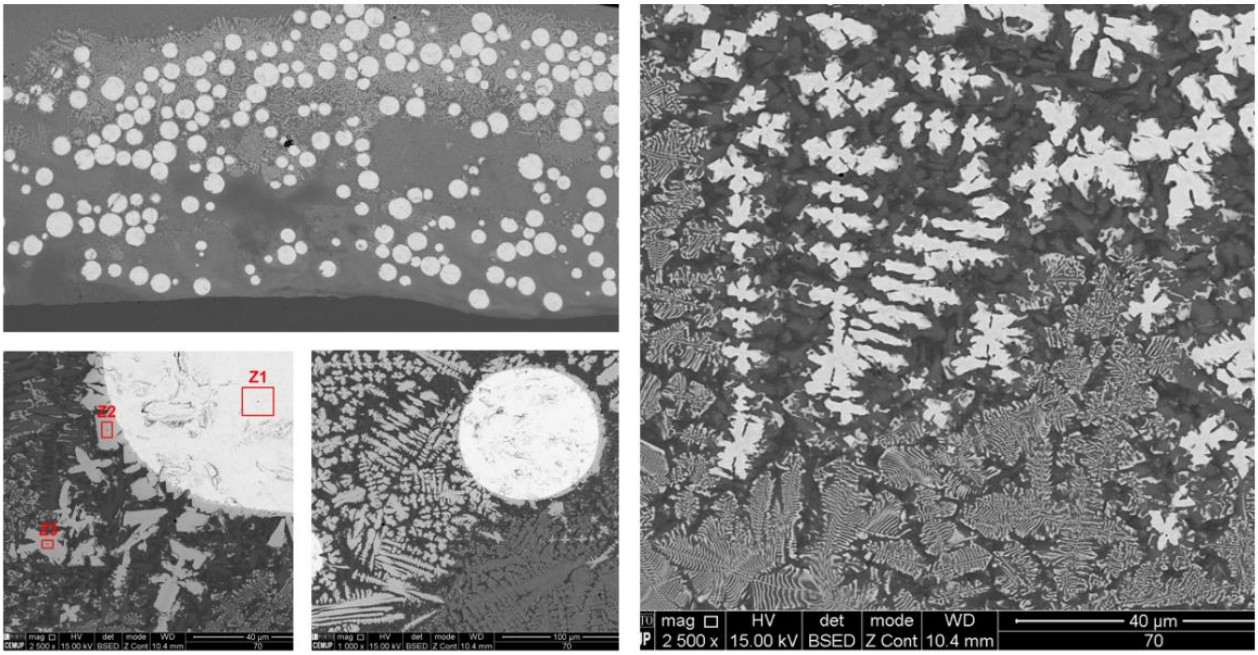

Figure 27 - SEM images of sample 70, alongside EDS's analysis zones.

Table 10 - Chemical analysis of phases in coating/wt-%, sample 70.

Symbol	W	C	Cr	Fe	Ni	Mo	Phase
Z1	98.40	1.60	-	-	-	-	WC
Z2	61.64	1.15	8.15	1.83	17.00	10.23	W_2C
Z3	57.25	1.02	10.03	2.28	18.42	10.96	W_2C

As it can be seen in Figure 25, an EDS analysis was directed in the boundaries of WC powder spheres, in order to assess their dissolution. Again, since Z1 is located inside the sphere, most of the chemical content consists of tungsten. The eutectic phases identified as zones Z2 and Z3, which are also present in most of the microstructure shown in Figure 27's top left, consist of W_2C. Although it may seem similar to what was observed in the previous sample (10), the content of W_2C here appeared to decrease, being replaced by a new phase getting formed in areas of the microstructure in which sphere agglomeration is lower. Here, the dissolution process caused the formation of a fishbone-like structure, typical for topologically close-packed (TCP) phases, which are generally found in nickel alloys after heat treatment. The nature of laser cladding technology and the addition of ceramic induced their formation **[76].**

Figures 28 and 29 are relative to sample 74, the lowest content of tungsten carbide in the metal matrix coating (40%). Figure x6 assembles the chosen zones, 1 to 7, that were further analysed with aid of EDS. The results are shown in Table 11.

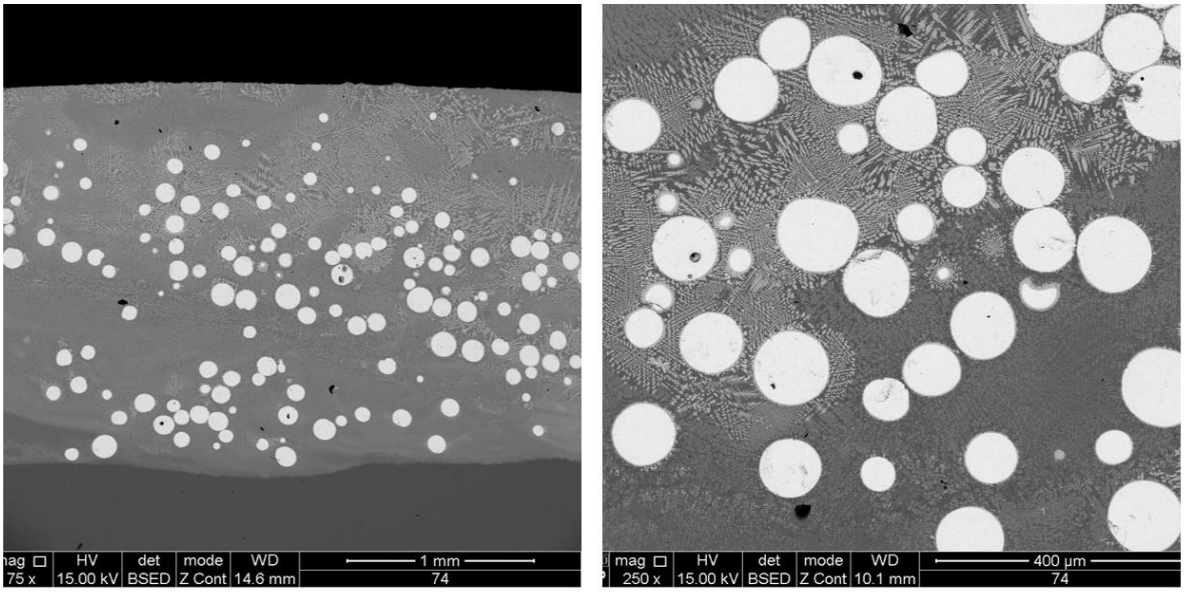

Figure 28 - SEM images of sample 74, alongside EDS's analysis zones.

The left picture in Figure 28 makes it visible that, similarly to what happened in the previous sample (70), the white phased areas in the boundaries of the tungsten carbide powder spheres reduced drastically, giving up their place in the microstructure to what it seems to be, again, topologically close-packed phases (TCP).

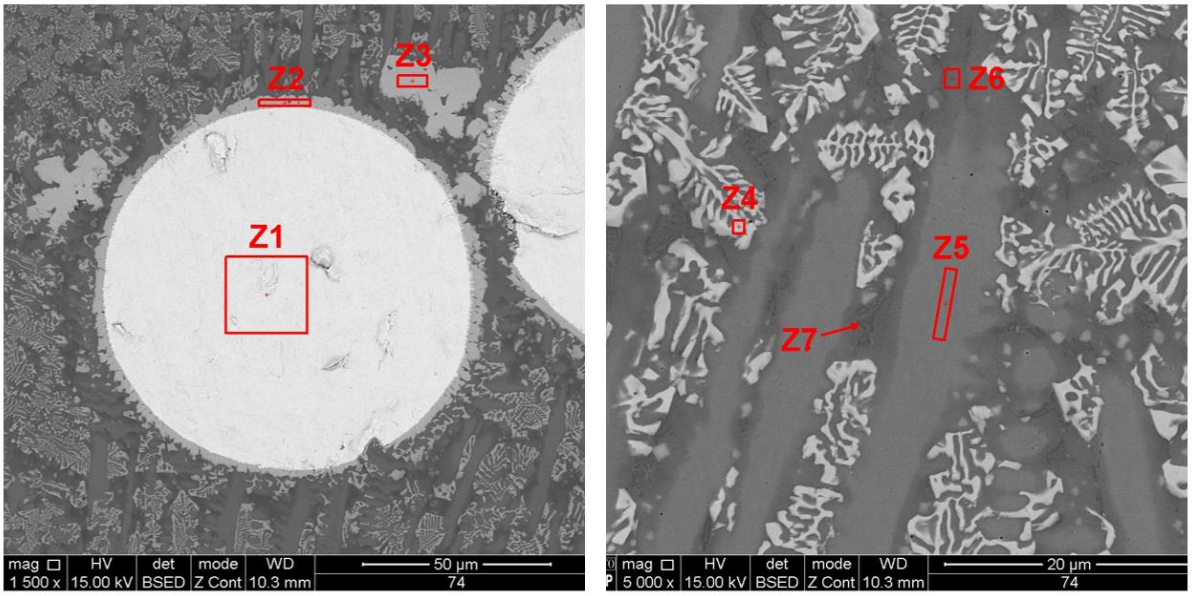

Figure 29 - EDS's analysis zones for sample 74.

Table 11 - Chemical analysis of phases in coating/wt-%, sample 74.

Symbol	W	C	Cr	Fe	Ni	Mo	Nb	Phase
Z1	98.88	1.12	-	-	-	-	-	WC
Z2	57.01	0.82	9.70	1.16	18.54	12.77	-	W_2C
Z3	58.69	0.65	8.93	1.11	18.98	11.65	-	W_2C
Z4	35.89	1.35	14.31	2.02	27.75	13.90	4.78	TCP phase
Z5	16.69	0.58	15.11	3.57	57.73	4.90	1.42	γ-Ni matrix
Z6	8.85	0.71	21.06	3.21	60.38	5.80	-	γ-Ni matrix
Z7	11.03	2.35	48.87	1.85	21.46	14.44	-	$Cr_{23}C_6$

The conducted EDS analysis of the zones displayed in Figure 29 revealed, yet again, that zones Z1, Z2 and Z3 consist of WC, and its direct dissolution product, the W_2C phase. This time, the fishbone-like structure known as TCP was chemically examined, Z4, revealing that this phase presents some rather high content of Mo, Nb and C. In the boundaries of the TCP phase, zones Z5 and Z6 assess the chemical composition of dark-phased columnar dendrites, which by the low tungsten content (suggesting the element's diffusion) and high percentage of main alloying elements (Ni and Cr) is suggested to be the γ matrix. Lastly, the Z7 spot was chosen in between γ matrix dendrites. The EDS analysis revealed that the last one has the highest carbon content in the microstructure, which added to the fact that Cr is present in its majority, makes it possible that this phase consists of $Cr_{23}C_6$, one of the secondary carbides that were a possible consequence of the WC dissolution **[76].**

4.5. Tribology Tests

The track area of samples processed with different parameters was examined, to then analyse their influence on wear resistance. The increase in measured area corresponds to a decrease in wear resistance.

4.5.1 Tungsten Carbide Variation

Figure 30 portrays the measured areas for samples 10, 70 and 74. These were obtained with the same laser power, transverse speed and overlap ratio, only varying the tungsten carbide percentage in the matrix: 60, 50 and 40, accordingly. As it was previously acknowledged with the SEM images of this same group of samples, Figure 25, the distribution of WC was less homogeneous as the percentage of powder in the composite decreased. These same images show that the upper parts of the coating display less quantity of WC than its core. With that being said, and as it was expected, sample 10 showed the highest wear resistance, with a measured area of 14.23mm^2. While looking at its microstructure in Figure 30, the presence of tungsten carbide spheres is highly noticeable. The theory of having higher resistance with the increase of WC content was not demonstrated when looking at the measured areas for the two other samples: sample 74, the one with the lower ceramic content, prevailed over sample 70. This is possibly due to the fact that less spheres were located in the upper part of the coating, the part that was ultimately analysed during these tests. Also, the existence of microstructural products of the WC dissolution in the coating, such as W_2C and TCP phase, may have been less prevalent in sample 70.

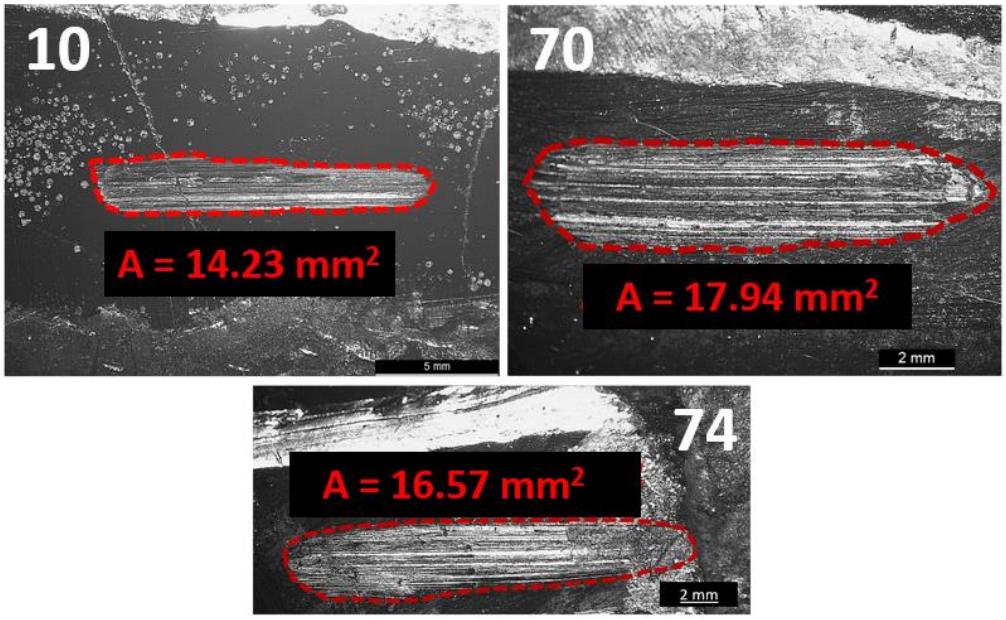

Figure 30 - Measured track areas for samples with different %WC.

4.5.2 Overlap Degree Variation

Figure 31 portrays the measured areas for samples 80, 72 and 76. These were obtained with the same laser power, transverse speed and tungsten carbide percentage, only varying the degree of overlap: 40, 30 and 20%, accordingly. Similarly to what was viewed during hardness testing, the increase in overlap, which then caused a decrease in measured hardness, resulted in decreasing wear resistance, while comparing samples 72 and 76. The unexpected result was the measured wear track of sample 80, 15.10mm^2: being the one with the highest value of overlap, according to the theory, should be exhibiting the lowest resistance to wear. This fact can be explained by visualization of its microstructure in Figure 31, in which the presence of tungsten carbide spheres is highly noticeable.

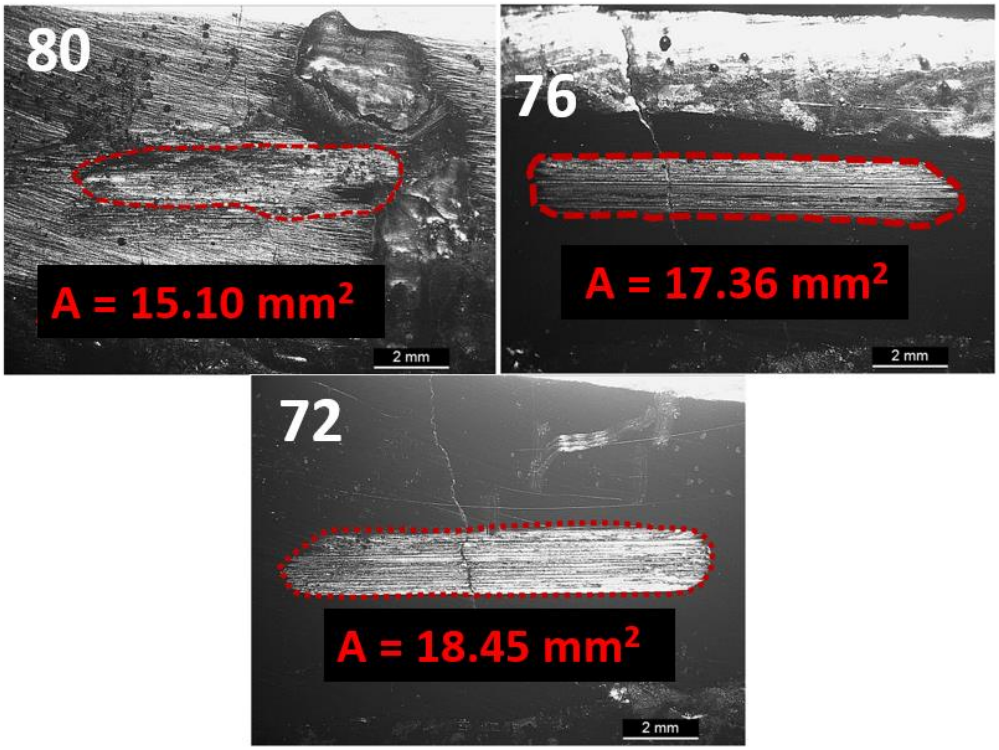

Figure 31 - Measured track areas for samples with different overlaps.

4.5.3 Laser Power Variation

Figure 32 displays the measured areas for samples 72 and 74. These were obtained with the same tungsten carbide percentage, transverse speed and overlap ratio, only varying the laser power: 10450 and 12100, respectively. The results were coherent with what was expected, as the sample produced with higher laser power showed higher wear resistance. The higher energy input leads to more tungsten carbide dissolution, which promotes the formation of the before mentioned hard phases in the microstructure, diminishing the measured area. Also, higher laser power promotes finer microstructure, as the solidification speed increases.

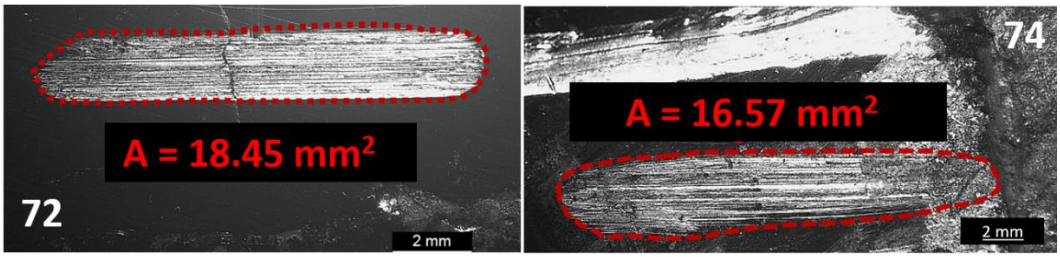

Figure 32 - Measured track areas for samples with different laser power.

Chapter 5

Conclusions and Future Work

Throughout this work, multiple illations resulted from the variation of the processing parameters of the LC technology, both regarding intermixing between the coating and the substrate, microstructure, and mechanical properties (hardness and wear resistance). These were:

- The increase in laser power, which implies the increase of energy input, culminated in more dilution in the specimen, as the three samples processed with 12100 W (70, 74, 10) displayed the highest measured values. When it comes to hardness and wear resistance, by comparing samples 72 and 74: the increase in energy per unit time of laser (10450 to 12100 W) resulted in a direct escalation of the measured hardness values (984 to 1053 HV) and less worn area (18.45 to 16.57 $mm^{2)}$. The higher energy input leads to more tungsten carbide dissolution, which promotes the formation of hard phases in the microstructure, explaining the hardness and wear resistance rise. The substrates' hardness also increased, due to the material intermixing with the coating (even if slight) and from the resultant heat of the process, which acted as a heat treatment for the specimens.

- The increase of tungsten carbide percentage in the matrix, responsible for reducing the thermal conductivity of the composite, diminishes the possibility for causing dilution. This fact was corroborated by the results, as the dilution was less in the composites with more WC content: samples 10, 70, and 74, displayed percentages of 2.54, 3.33, and 3.78, respectively. SEM/EDS analysis revealed that the increase in WC content helped achieve a more homogeneous distribution of the carbides in the microstructure. Also, the increasing content of tungsten carbide potentiated the formation of secondary carbides, such as W_2C and M_6C, and favoured the reduction of TCP phase formation. This fact, allied to the increase of WC by itself in the microstructure, caused an enhancement of hardness and wear resistance: sample 74 - 1053 HV, and 16.57 mm^2; sample 10 - 1122 HV, and 14.23 mm^2.

- The increase of the overlap degree reduces the hypothesis of mixing between the feedstock and the substrate. By assessing the results of the dilution measured in samples 76, 72, and 80, the increase of overlap was responsible for reducing the level of dilution (2.16, 2.11, and 1.20%, respectively). Regarding mechanical properties, the overlap increase results in an increase of solidification time, which translates into a decrease of hardness. This was also viewed in the results of samples 76, 72, and 80 (1060, 984, and 914 HV). In tribology testing, the results collided with what was expected in theory, as the sample with the highest overlap of the group, 80, had the lowest measured worn area, 15.10 mm^2.

From an overall results point of view:

- Least dilution was observed with sample 80, 1.20%.
- Highest hardness was observed with sample 10, 1122 HV.
- Best tribology test result belonged to sample 10, with a worn area of 14.23 mm^2.

With these values in mind, sample 10, which was ranked as the 7th best sample by Minitab, displayed the best tested mechanical properties. This can be explained by the existence of reinforcing hard particles in its microstructure in very high amount and, most importantly, their distribution within the matrix, as this sample exhibited the most homogeneous carbide distribution amongst the processed ones. Nevertheless, there was not a substantial difference in the mechanical properties, when compared to the rest of the samples, that would justify paying for the extra content of the tungsten carbide in the matrix, being that the last one is the more expensive component in the composite. There is still a long path to achieve crack-free clads with unmelted, and homogeneously distributed, reinforcing tungsten carbide in the matrix.

The variation of processing parameters and study of their interaction remains the core for achieving the wanted results for LC processing. Nevertheless, this work showed the importance of further study of WC quantification and distribution in the composite matrix, as a way of understanding its influence in the mechanical properties. Also, it would be interesting to assess the composite wear resistance when exposed to a corrosive medium, and conduct further XRD and EBSD analysis.

References

[1] Mussatto A., Ahad I., Mousavian R., Delaure Y., Brabazon D. "Advanced production routes for metal matrix composites". 2020

https://doi.org/10.1002/eng2.12330

[2] Samal, Prasan K. Newkirk, Joseph W. (2015). *ASM Handbook, Volume 07 - Powder Metallurgy (2015)*. ASM International. Retrieved from https://app.knovel.com/hotlink/toc/id:kpASMHVP1R/asm-handbook-volume-07/asm-handbook-volume-07

[3] Liaoyuan Chen, Tianbiao Yu, Xin Chen, Yu Zhao, Chuang Guan,"Process optimization, microstructure and microhardness of coaxial laser cladding TiC reinforced Ni-based composite coatings",Optics & Laser TechnologyVolume 152,2022,108129,ISSN 0030-3992, https://doi.org/10.1016/j.optlastec.2022.108129

[4] Fraunhofer IWS, ed., Annual Report 2021/2022 - Fraunhofer IWS Dresden, 2021. [Online]. Available at: Annual reports - Fraunhofer IWS. Accessed on 2022-05-30

[5] K.P. Cooper, J.D. Ayer, in: Proceedings of the Laser Surface Modification Conference, New Orleans, LA, 1988, pp. 115–131.

[6] Olga Vayena, Charalabos Doumanidis, Rajesh Ranganathan, Teiichi Ando, "Welding Methods for Production of MMC Coatings Using Particulate-Cored Wire Precursors", Journal of Manufacturing Processes, Volume 7, Issue 2, 2005, Pages 130-139,ISSN 1526-6125, https://doi.org/10.1016/S1526-6125(05)70090-6.

[7] https://www.fortunebusinessinsights.com/protective-coatings-market-102942 Accessed on 2022-05-30

[8] Park SJ, Seo MK. *Interface Science and Composites*. Vol. 18. First edition, Amsterdam: Academic Press; 2011

[9] Nichols RW. *Advanced Materials by Design: New Structural Materials Technologies*. Washington, DC: DIANE Publishing; 1988.

[10] Reddy BSB, Das K, Das S. "A review on the synthesis of in situ aluminum based composites by thermal, mechanical and mechanical–thermal activation of chemical reactions". *J Mater Sci*. 2007;42(22):9366-9378. DOI:10.1007/s10853-007-1827-z

[11] Aikin RM. The mechanical properties of in-situ composites. *JOM*. 1997;49(8):35-39.

[12] Yi XS, Du S, Zhang L. *Composite Materials Engineering: Different Types of Composite Materials*. Vol. 2. Singapore: Springer; 2017.

[13] Banerjee R, Manna I. *Ceramic Nanocomposites*. Cambridge, UK: Woodhead Publishing; 2013.

[14] Thandalam SK, Ramanathan S, Sundarrajan S. "Synthesis, microstructural and mechanical properties of ex situ zircon particles (ZrSiO4) reinforced metal matrix composites (MMCs): A review". *J Mater Res Technol*. 2015;4(3):333-347. https://doi.org/10.1016/j.jmrt.2015.03.003

[15] Natarajan N, Krishnaraj V, Davim JP. *"Metal Matrix Composites: Synthesis, Wear Characteristics, Machinability Study of MMC Brake Drum"*. New York: Springer; 2014.

[16] Saboori A, Moheimani SK, Dadkhah M, Pavese M, Badini C, Fino P. "An overview of key challenges in the fabrication of metal matrix nanocomposites reinforced by graphene nanoplatelets". *Metals*. 2018;8(3):172. DOI:10.3390/met8030172

[17] Balasubramanian M. *Composite Materials and Processing*. Florida: CRC Press; 2013.

[18] Pramanik A, Littlefair G. "Fabrication of nano-particle reinforced metal matrix composites". *Adv Mater Res*. 2013;651:289-294. DOI:10.4028/www.scientific.net/AMR.651.289

[19] https://www.iws.fraunhofer.de/en/newsandmedia/press_releases/2022/press-release_2022-06_hiclad_laserline.html. Accessed on 2022-05-30

[20] Shaowei Zhou, Tianyu Xu, Chang Hu, Han Wu, Huailiang Liu, Xiuquan Ma, "Utilizing carbon nanotubes in ceramic particle reinforced MMC coatings deposited by laser cladding with Inconel 625 wire",Journal of Materials Research and Technology, Volume 13, 2021, Pages 2026-2042, ISSN 2238-7854. https://doi.org/10.1016/j.jmrt.2021.06.028.

[21] R. Jäckel, "Laser-lexikon," Fraunhofer Institute for Material and Beam Technology, 2015. Accessed on 2022-05-30

[22] Janne Nurminen, Jonne Näkki, Petri Vuoristo, "Microstructure and properties of hard and wear resistant MMC coatings deposited by laser cladding", International Journal of Refractory Metals and Hard Materials, Volume 27, Issue 2, 2009, Pages 472-478, ISSN 0263-4368, https://doi.org/10.1016/j.ijrmhm.2008.10.008.

[23] Arif, Z.U., Khalid, M.Y., Rehman, E., Ullah, S., Atif, M., Tariq, A. 2021. "A review on laser cladding of high-entropy alloys, their recent trends and potential applications". Journal of Manufacturing Processes 68: 225-273. https://doi.org/10.1016/j.jmapro.2021.06.041

[24] L. AG, "Linde: Shielding gases- overview brochure," tech. rep., Linde AG. Accessed on 2022-05-30

[25] Shaowei Zhou, Tianyu Xu, Chang Hu, Han Wu, Huailiang Liu, Xiuquan Ma, Effect of different topologies on microstructure and mechanical properties of multilayer coatings deposited by laser cladding with Inconel 625 wire, Surface and Coatings Technology, Volume 421, 2021, 127299, ISSN 0257-8972, https://doi.org/10.1016/j.surfcoat.2021.127299.

[26] Jianjun Shi, Ping Zhu, Geyan Fu, Shihong Shi, Geometry characteristics modeling and process optimization in coaxial laser inside wire cladding, Optics & Laser Technology, Volume 101, 2018, Pages 341-348, ISSN 0030-3992, https://doi.org/10.1016/j.optlastec.2017.10.035.

[27] J.C. Heigel, M.F. Gouge, P. Michaleris, T.A. Palmer, Selection of powder or wire feedstock material for the laser cladding of Inconel® 625, Journal of Materials Processing Technology, Volume 231, 2016, Pages 357-365, ISSN 0924-0136, https://doi.org/10.1016/j.jmatprotec.2016.01.004.

[28] Marvin Leingruber, "Entwicklung und Untersuchung von Hochleistungs-Laser-Auftragschweißköpfen mit draht- und bandförmigen Schweißzusatzwerkstoffen", 2021

[29] Jyotsna Dutta Majumdar, Indranil Manna. "Laser-assisted fabrication of materials", volume 161.Springer Science & Business Media, 2012.

[30] Fraunhofer IWS. Powder nozzles for lateral feed. URL https://www.iws.fraunhofer.de/en/business_fields/surface_treatment/laser_cladding/system_technology/cyclone_powder_nozzle.html. Accessed on 2022-05-30.

[31] A. Weisheit, A. Gasser, G. Backes, T. Jambor, N. Pirch, and K. Wissenbach, "Direct laser cladding, current status and future scope of application," in Laser-assisted fabrication of materials, pp. 221–240, Springer, 2013.

[32] A Weisheit, G Backes, R Stromeyer, A Gasser, K Wissenbach, and R Poprawe. "Powder injection: the key to reconditioning and generating components using laser cladding". In Proceedings of International Congress on Advanced Materials, Their Processes and Applications, pages 1–7, 2001.

[33] Fraunhofer IWS. System engineering for powder-based laser cladding, . URL https://www.ilt.fraunhofer.de/content/dam/ilt/en/documents/product_and_services/laser_material_processing/B_System_Engineering_for_Powder-Based_Laser_Cladding_2013.pdf. Accessed on 2022-05-30.

[34] H. J. Fahrenwaldt, V. Schuler, J. Twrdek, and H. J. Fahrenwaldt, Praxiswissen Schweißtechnik: Werkstoffe, Prozesse, Fertigung, 5th ed. Wiesbaden: Springer Vieweg, 2014.

[35] Waheed U.I. Haq Syed, Lin Li. "Effects of wire feeding direction and location in multiple layer diode laser direct metal deposition". Appl. Surface Sci. (2005), pp. 518-524, https://doi.org/10.1016/j.apsusc.2005.03.039

[36] R. Vilar. Laser cladding J. Laser Appl., 11 (1999), pp. 64-79 https://doi.org/10.2351/1.521888

[37] Fraunhofer IWS, LASER PROCESSING OPTIC COAXwire Cladding - repair and additive manufacturing using wire as feedstock material, 2018

[38] Ocylok, S., Leichnitz, M., Thieme, S., Nowotny, S. 2016. "Investigations on laser metal deposition of stainless steel 316L with coaxial wire feeding".

[39] Oerlikonmetco, "Frequently asked questions: Laser cladding," tech. Rep.

[40] "Laser Cladding with hardmetals for application in forming dies", António José Pontes Silva, 2017

[41] Hofman, J. T. (2009). *Development of an observation and control system for industrial laser cladding*. University of Twente.

[42] B. Oberländer and E. Lugscheider, "Comparison of properties of coatings produced by laser cladding and conventional methods," Materials Science and Technology, vol. 8, no. 8, pp. 657–665, 1992.

[43] F. P. NEME ˇ CEK, S., "The corrosion resistance of laser-cladded layers," ˇ Conference of Laser Application in Industry Plzen, 16-18/3/2015.

[44] Wei Ya. "Laser materials interactions during cladding: analyses on clad formation, thermal cycles, residual stress and defects". PhD thesis, University of Twente, 10 2015.

[45] António Borges Correia, "Seleção e otimização dos parâmetros do processo de Laser Cladding para a reparação de componentes", 2018

[46] M. vostˇrák, M. Hruška, š. Houdková, and E. Smazlová, "Coaxial laser cladding of stellite: Analysis of process parametres," in Proc. of, vol. 23, pp. 21–23

[47] U. De Oliveira, V. Ocelik, and J. T. M. De Hosson, "Analysis of coaxial laser cladding processing conditions," Surface and Coatings Technology, vol. 197, no. 2, pp. 127–136, 2005. https://doi.org/10.1016/j.surfcoat.2004.06.029

[48] Xingyun Yang, Leilei Wang, Zhuanni Gao, Qiang Wang, Mingzhen Du, Xiaohong Zhan, "WC distribution, microstructure evolution mechanism and microhardness of a developed Ti-6Al-4 V/WC MMC coating fabricated by laser cladding", Optics & Laser Technology, Volume 153, 2022, 108232, ISSN 0030-3992, https://doi.org/10.1016/j.optlastec.2022.108232.

[49] T. E. Abioye, J. Folkes, and A. T. Clare, "A parametric study of Inconel 625 wire laser deposition," J. Mater. Process. Technol. **213**, 2145–2151 (2013). https://doi.org/10.1016/j.jmatprotec.2013.06.007

[50] T.E. Abioye, J. Folkes, A.T. Clare, A parametric study of Inconel 625 wire laser deposition, Journal of Materials Processing Technology, Volume 213, Issue 12, 2013, Pages 2145-2151, ISSN 0924-0136, https://doi.org/10.1016/j.jmatprotec.2013.06.007.

[51] G.P. Dinda, A.K. Dasgupta, J. Mazumder, "Laser aided direct metal deposition of Inconel 625 superalloy: Microstructural evolution and thermal stability", Materials Science and Engineering: A, Volume 509, Issues 1–2, 2009, Pages 98-104, ISSN 0921-5093, https://doi.org/10.1016/j.msea.2009.01.009.

[52] Mohammad Naghiyan Fesharaki, Reza Shoja-Razavi, Hojjat Allah Mansouri, Hossein Jamali, "Microstructure investigation of Inconel 625 coating obtained by laser cladding and TIG cladding methods", Surface and Coatings Technology, Volume 353, 2018, Pages 25-31, ISSN 0257-8972, https://doi.org/10.1016/j.surfcoat.2018.08.061.

[53] U. de Oliveira, V. Ocelík, J.Th.M. De Hosson, "Residual stress analysis in Co-based laser clad layers by laboratory X-rays and synchrotron diffraction techniques", Surface and Coatings Technology, Volume 201, Issues 3–4, 2006, Pages 533-542, ISSN 0257-8972, https://doi.org/10.1016/j.surfcoat.2005.12.011.

[54] A. Zikin, M. Antonov, I. Hussainova, L. Katona, A. Gavrilović. Tribol. Int. 68, 45 (2013). Crossref

[55] A.V. Makarov, Y.S. Korobov, N.N. Soboleva, Y.V. Khudorozhkova, A.A. Vopneruk, P. Balu, M. Barbosa, I.Y. Malygina, S.V. Burov, A.K. Stepchenkov. "Wear-resistant nickel-based laser clad coatings for high-temperature applications". Lett. Mater., 2019, 9(4) 470-474. https://doi.org/10.22226/2410-3535-2019-4-470-474

[56] Balu, P., Hamid, S. & Kovacevic, R. An Experimental Study on Slurry Erosion Resistance of Single and Multilayered Deposits of Ni-WC Produced by Laser-Based Powder Deposition Process. *J. of Materi Eng and Perform* 22, 3398–3413 (2013). https://doi.org/10.1007/s11665-013-0620-1

[57] Ortiz, A., A. García, M. Cadenas, M. R. Fernández, and J. M. Cuetos. "WC particles distribution model in the cross-section of laser cladded NiCrBSi+WC coatings, for different wt% WC". Surface and Coatings Technology, Vol. 324, 2017, pp. 298–306. https://doi.org/10.1016/j.surfcoat.2017.05.086

[58] Tobar, M. J., C. Álvarez, J. M. Amado, G. Rodríguez, and A. Yáñez. "Morphology and characterization of laser clad composite NiCrBSi-WC coatings on stainless steel". Surface and Coatings Technology, Vol. 200, No. 22-23, 2006, pp. 6313–6317. https://doi.org/10.1016/j.surfcoat.2005.11.093

[59] Li, F.Q., X. Y. Feng, Y. B. Chen. "Effect of WC content on microstructure of WC/Ni60A laser cladding layer". Chin. J. Las, Vol. 43, No. 1, 2016, pp. 0403009-1-0403009-7.

[60] Ma, Q. S., Y. J. Li, J. Wang, and K. Liu. "Investigation on cored-eutectic structure in Ni60/WC composite coatings fabricated by wide-band laser cladding". Journal of Alloys and Compounds, Vol. 645, 2015, pp. 151–157. https://doi.org/10.1016/j.jallcom.2015.04.136

[61] Guo, C., J. M. Chen, J. S. Zhou, J. R. Zhao, L. Q. Wang, Y. J. Yu, et al. "Effects of WC-Ni content on microstructure and wear resistance of laser cladding Ni based alloys coating". Surface and Coatings Technology, Vol. 206, No. 8-9, 2012, pp. 2064–2071. DOI:10.1016/j.surfcoat.2011.06.005

[62] Zhou, S. F., J. B. Lei, X. Q. Dai, J. B. Guo, Z. J. Gu, and H. B. Pan. "A comparative study of the structure and wear resistance of NiCrBSi/50 wt.% WC composite coatings by laser cladding and laser induction hybrid cladding." International Journal of Refractory Metals and Hard Materials, Vol. 60, 2016, pp. 17–27. https://doi.org/10.1016/j.ijrmhm.2016.06.019

[63] T.E. Abioye, P.K. Farayibi, D.G. McCartney, A.T. Clare, "Effect of carbide dissolution on the corrosion performance of tungsten carbide reinforced Inconel 625 wire laser coating", Journal of Materials Processing Technology, Volume 231,2016,Pages 89-99,ISSN 0924-0136, https://doi.org/10.1016/j.jmatprotec.2015.12.023.

[64] S.W Huang, M Samandi, M Brandt, "Abrasive wear performance and microstructure of laser clad WC/Ni layers", Wear, Volume 256, Issues 11–12, 2004, Pages 1095-1105, ISSN 0043-1648, https://doi.org/10.1016/S0043-1648(03)00526-X.

[65] Z. Liu, J. Cabrero, S. Niang, Z.Y. Al-Taha, "Improving corrosion and wear performance of HVOF-sprayed Inconel 625 and WC-Inconel 625 coatings by high power diode laser treatments", Surface and Coatings Technology, Volume 201, Issues 16–17, 2007, Pages 7149-7158, ISSN 0257-8972, https://doi.org/10.1016/j.surfcoat.2007.01.032.

[66] T. Liyanage, G. Fisher, A.P. Gerlich, "Microstructures and abrasive wear performance of PTAW deposited Ni–WC overlays using different Ni-alloy chemistries", Wear, Volumes 274–275, 2012, Pages 345-354, ISSN 0043-1648, https://doi.org/10.1016/j.wear.2011.10.001.

[67] https://durmat.com/en/products/tungsten-carbide-and-its-derivatives/ Accessed on 2022-05-30

[68] https://matmatch.com/learn/material/inconel-625 Accessed on 2022-05-30

[69] https://www.azom.com/article.aspx?ArticleID=6022 Accessed on 2022-05-30

[70] Industrial Robots, Safety With KR C2 sr, KUKA Roboter GmbH Issued: 19.12.2011 Version: Sicherheit KR C2 sr V4 en. Accessed on 2022-05-30

[71] Dinse GmbH, FDE 100 L: Control system. [Online]. Available from: http://dinse.eu/produkte/?product_category=904&product=91

[72] P. Doan, 2022, "Erprobung von Multidraht beim Laserauftragschweißen"

[73] ISO 6507-1:2018 "Metallic materials — Vickers hardness test" Accessed on 2022-05-30

[74] Xingyun Yang, Leilei Wang, Zhuanni Gao, Qiang Wang, Mingzhen Du, Xiaohong Zhan, "WC distribution, microstructure evolution mechanism and microhardness of a developed Ti-6Al-4 V/WC MMC coating fabricated by laser cladding", Optics & Laser Technology, Volume 153, 2022, 108232, ISSN 0030-3992, https://doi.org/10.1016/j.optlastec.2022.108232.

[75] Saad M. S. Mukras, "Computer Simulation/Prediction of Wear in Mechanical Components", *Advances in Tribology*, vol. 2020, Article ID 8867351, 15 pages, 2020. https://doi.org/10.1155/2020/8867351

[76] Emanuelli, L.; Molinari, A.; Pellizzari, M. "Interaction between WC and Inconel 625 under Solid and Liquid State Sintering Conditions". Metals 2021, 11, 666. https://doi.org/10.3390/met11040666

[77] Huebner, J.; Kata, D.; Rutkowski, P.; Petrzak, P.; Kusiński, J. Grain-Boundary Interaction between Inconel 625 and WC during Laser Metal Deposition. *Materials* 2018, *11*, 1797. https://doi.org/10.3390/ma11101797

[78] D. Tanigawa, N. Abe, M. Tsukamoto, Y. Hayashi, H. Yamazaki, Y. Tatsumi & M. Yoneyama (2015) Effect of laser path overlap on surface roughness and hardness of layer in laser cladding, Science and Technology of Welding and Joining, 20:7, 601-606, DOI: 10.1179/1362171815Y.0000000044

[79] Wanlu Li, Riufeng Di, Ruwang Yuan, Heyu Song, Jianbo Lei, "Microstructure, wear resistance and electrochemical properties of spherical/non-spherical WC reinforced Inconel 625 superalloy by laser melting deposition", Journal of Manufacturing Processes, Volume 74, 2022, Pages 413-422, ISSN 1526-6125, https://doi.org/10.1016/j.jmapro.2021.12.045.

Appendix

Appendix 1 – Images of all produced samples


9
10
11
12
13
14


15
16
17
18
19
20
21
22


23
24
25
26
27
28
29
30

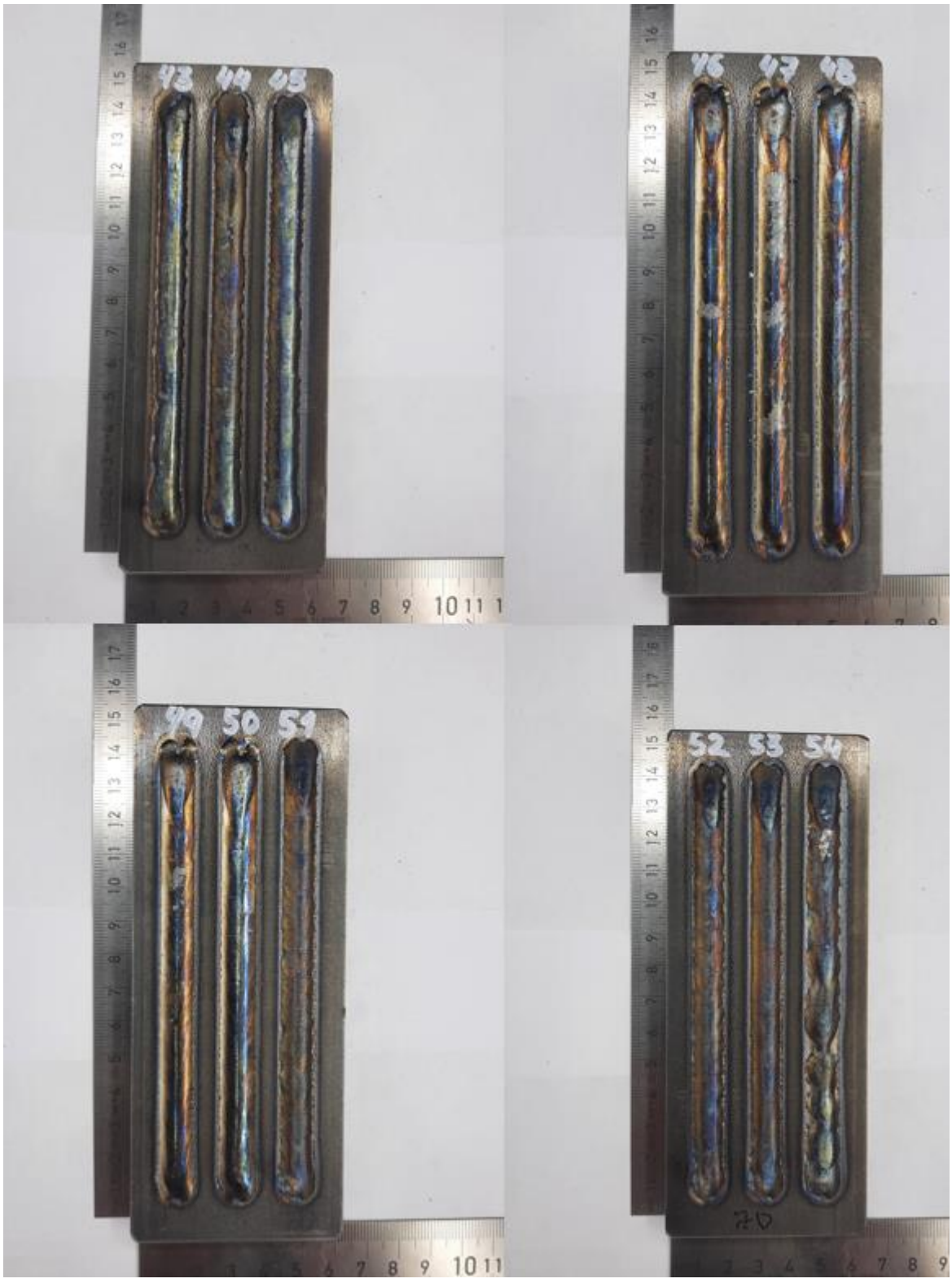
43 44 45
46 47 48
49 50 51
52 53 54


55
56
57
58
59
60
61
62
63
64
65


66
67
68
69
70
71
72
73


74
75
76
77
78
79
80
81


82
83
84
85
86
87
88


89
90
91
92
93
94
95
96


97
98
99
100
101
102
103
104


108
109
110
111
112
113
114
115

Appendix 2 - Hardness profiles

Sample 70

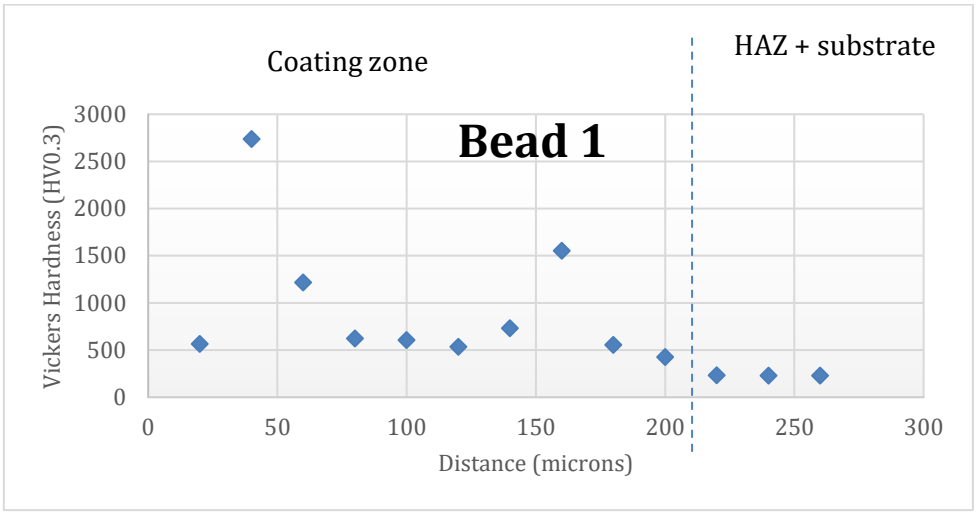

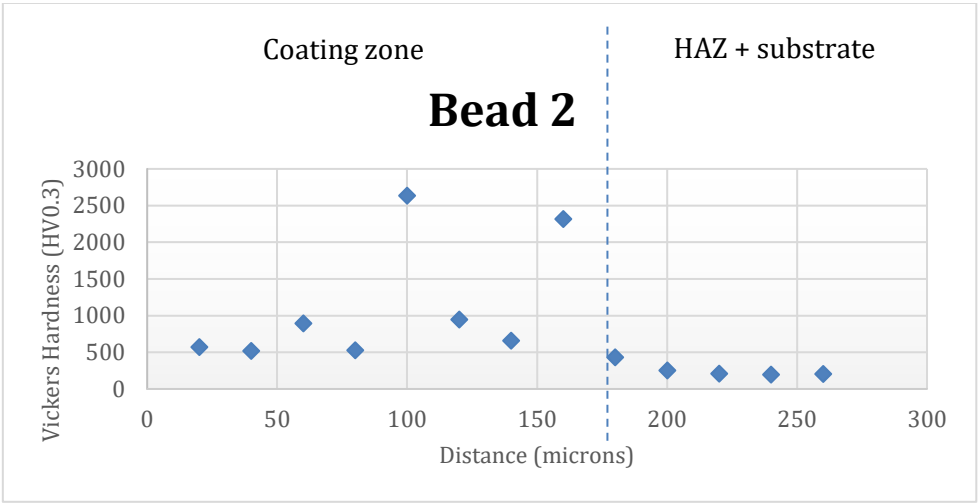

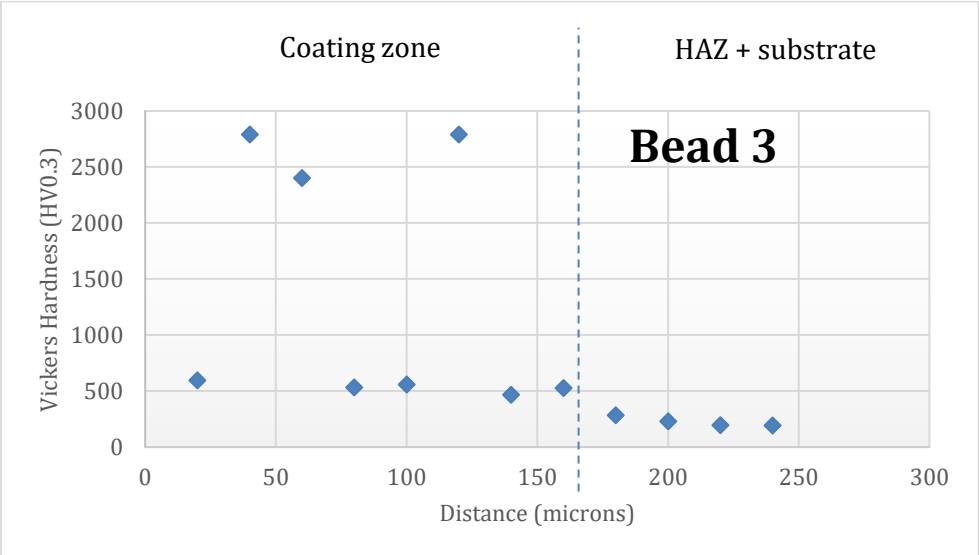

Sample 80

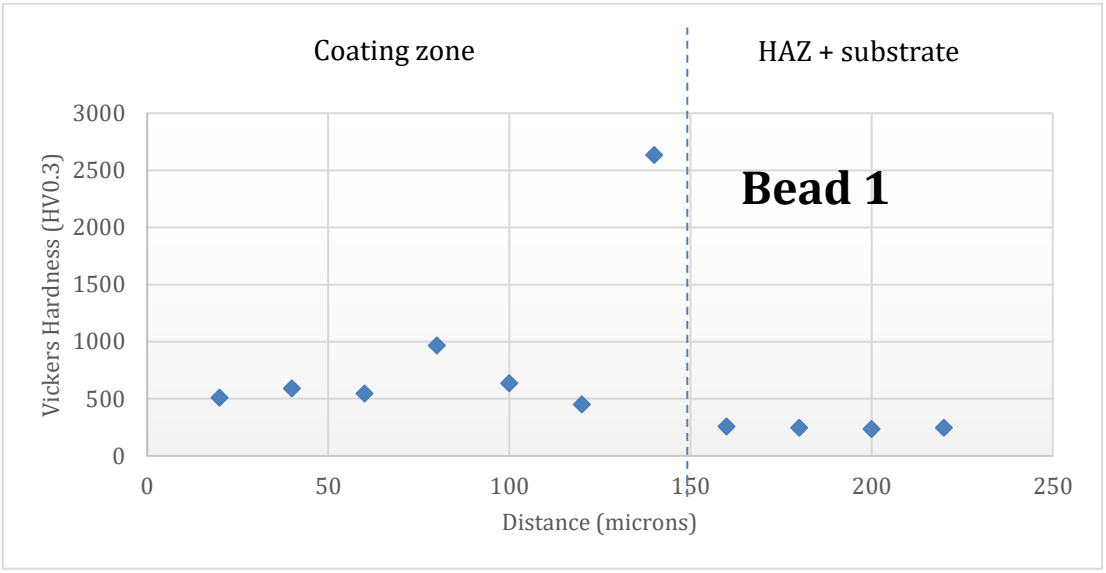
Coating zone
HAZ + substrate
Bead 1
Vickers Hardness (HV0.3)
3000
2500
2000
1500
1000
500
0
0
50
100
150
200
250
Distance (microns)

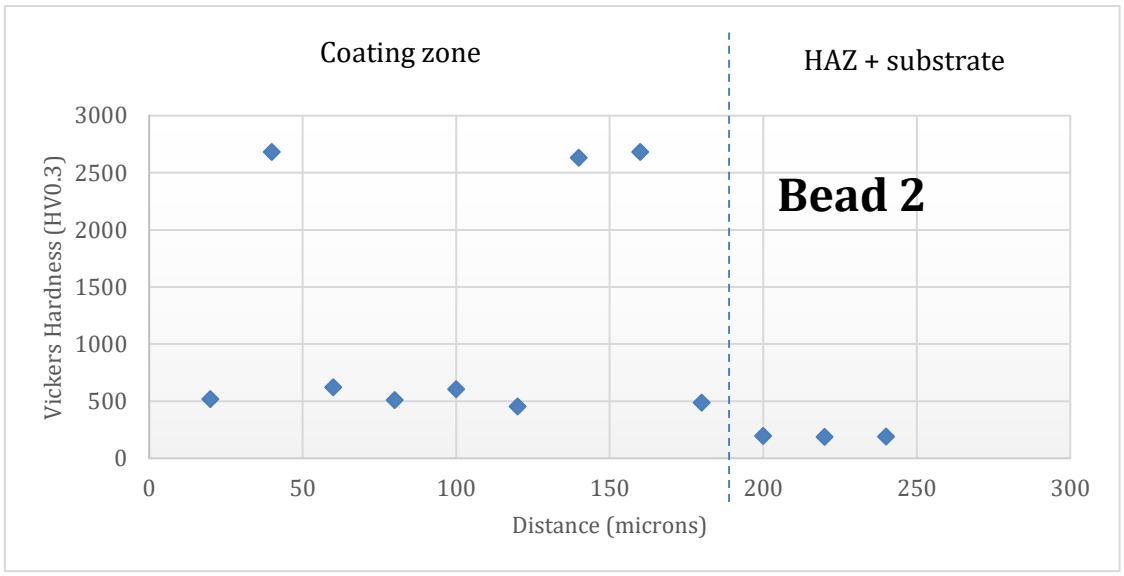
Coating zone
HAZ + substrate
Bead 2
Vickers Hardness (HV0.3)
3000
2500
2000
1500
1000
500
0
0
50
100
150
200
250
300
Distance (microns)

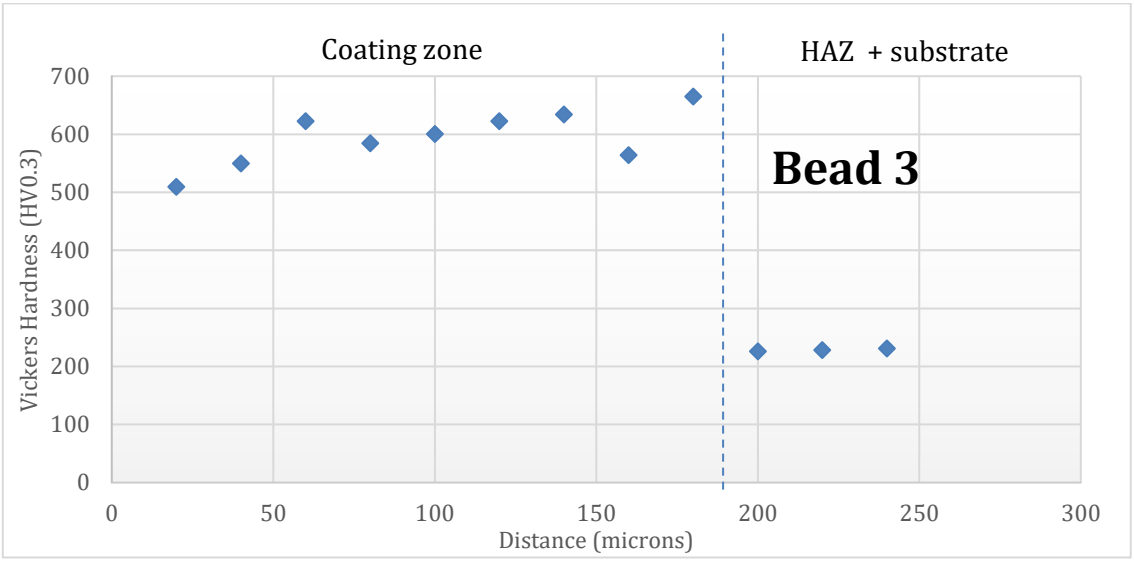
Coating zone
HAZ + substrate
Bead 3
Vickers Hardness (HV0.3)
700
600
500
400
300
200
100
0
0
50
100
150
200
250
300
Distance (microns)

Sample 10

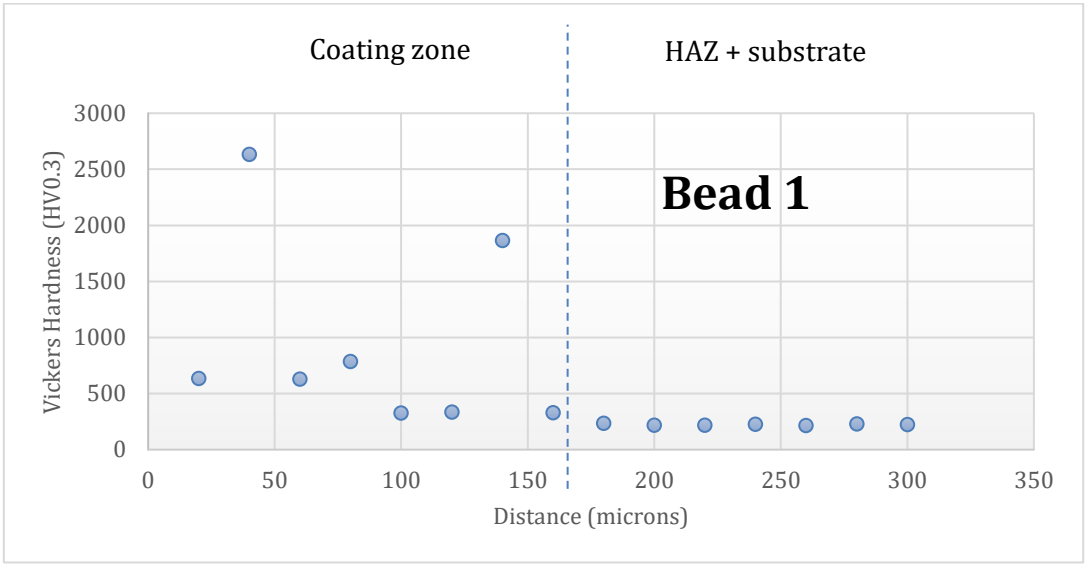
Coating zone
HAZ + substrate
Bead 1
Vickers Hardness (HV0.3)
3000
2500
2000
1500
1000
500
0
0
50
100
150
200
250
300
350
Distance (microns)

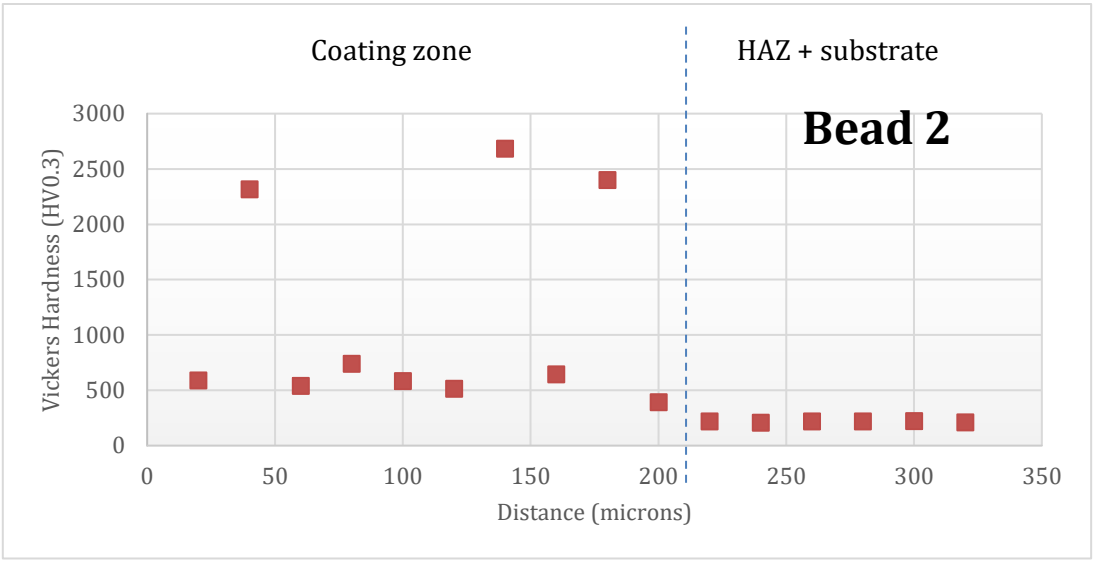
Coating zone
HAZ + substrate
Bead 2
Vickers Hardness (HV0.3)
3000
2500
2000
1500
1000
500
0
0
50
100
150
200
250
300
350
Distance (microns)

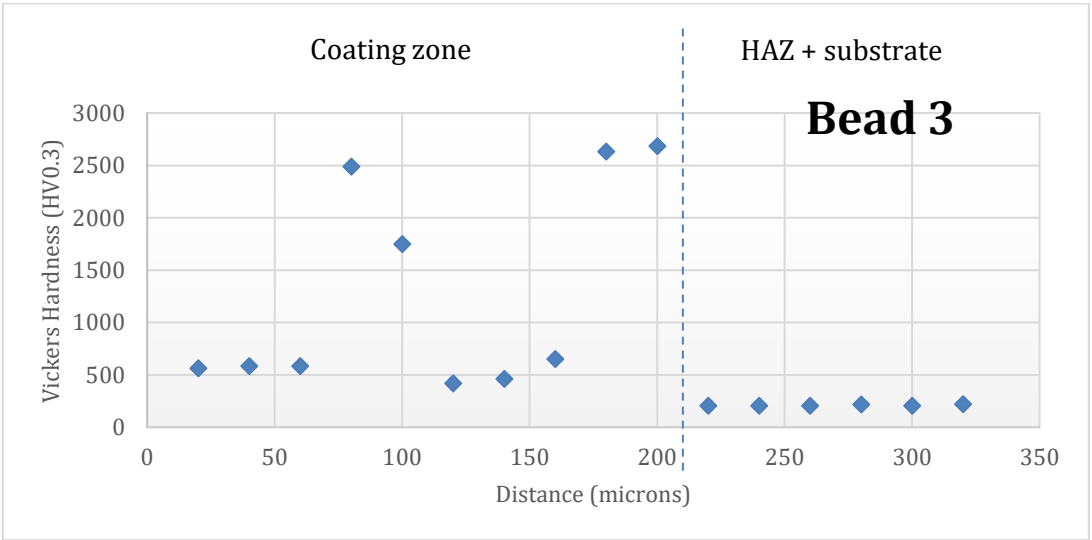
Coating zone
HAZ + substrate
Bead 3
Vickers Hardness (HV0.3)
3000
2500
2000
1500
1000
500
0
0
50
100
150
200
250
300
350
Distance (microns)

Sample 72

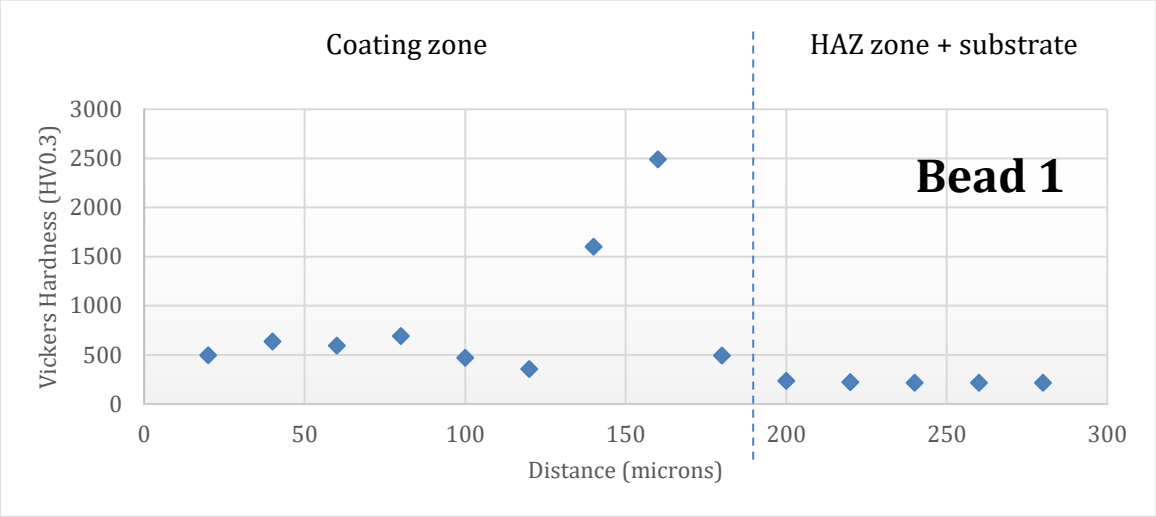
Coating zone
HAZ zone + substrate
Bead 1
Vickers Hardness (HV0.3)
3000
2500
2000
1500
1000
500
0
0
50
100
150
200
250
300
Distance (microns)

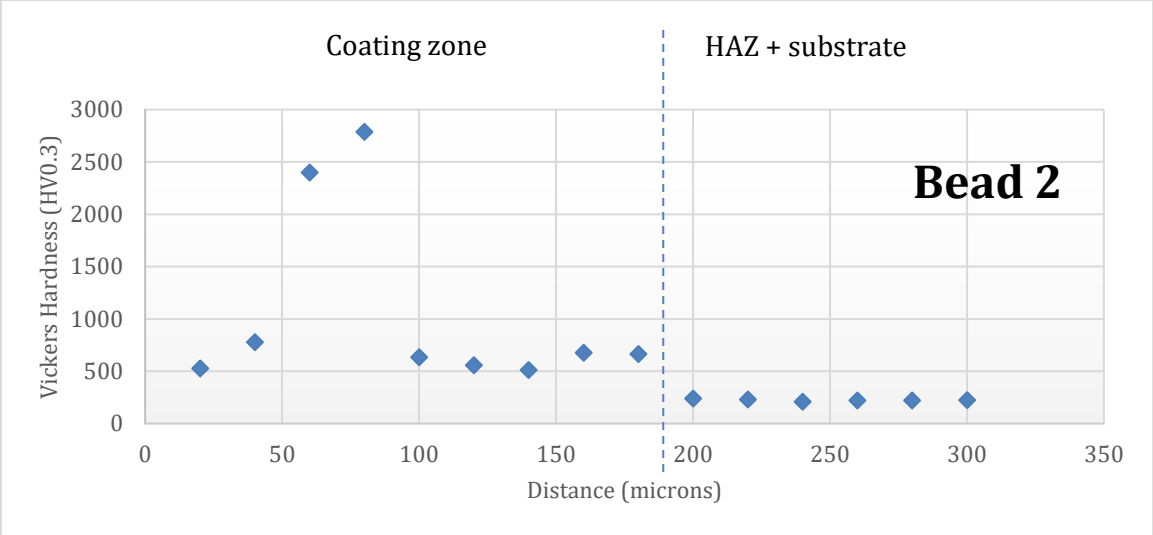
Coating zone
HAZ + substrate
Bead 2
Vickers Hardness (HV0.3)
3000
2500
2000
1500
1000
500
0
0
50
100
150
200
250
300
350
Distance (microns)

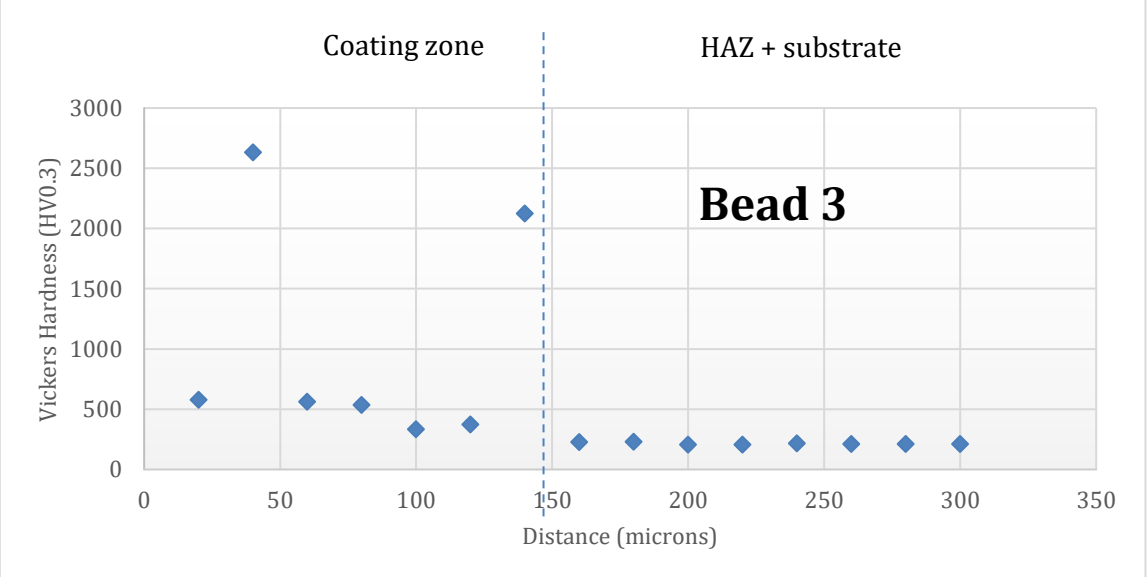
Coating zone
HAZ + substrate
Bead 3
Vickers Hardness (HV0.3)
3000
2500
2000
1500
1000
500
0
0
50
100
150
200
250
300
350
Distance (microns)

Sample 76

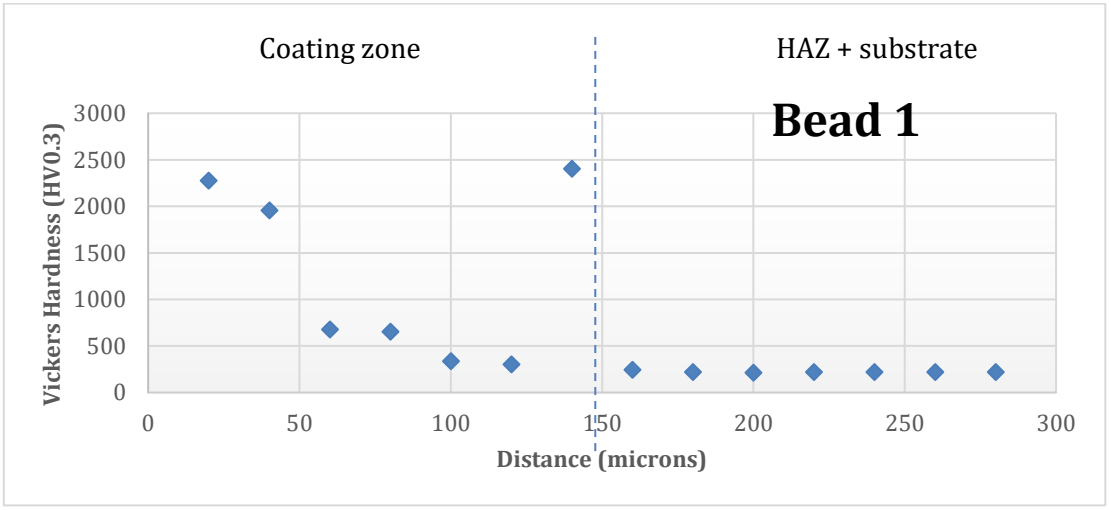
Coating zone
HAZ + substrate
Bead 1
Vickers Hardness (HV0.3)
3000
2500
2000
1500
1000
500
0
0
50
100
150
200
250
300
Distance (microns)

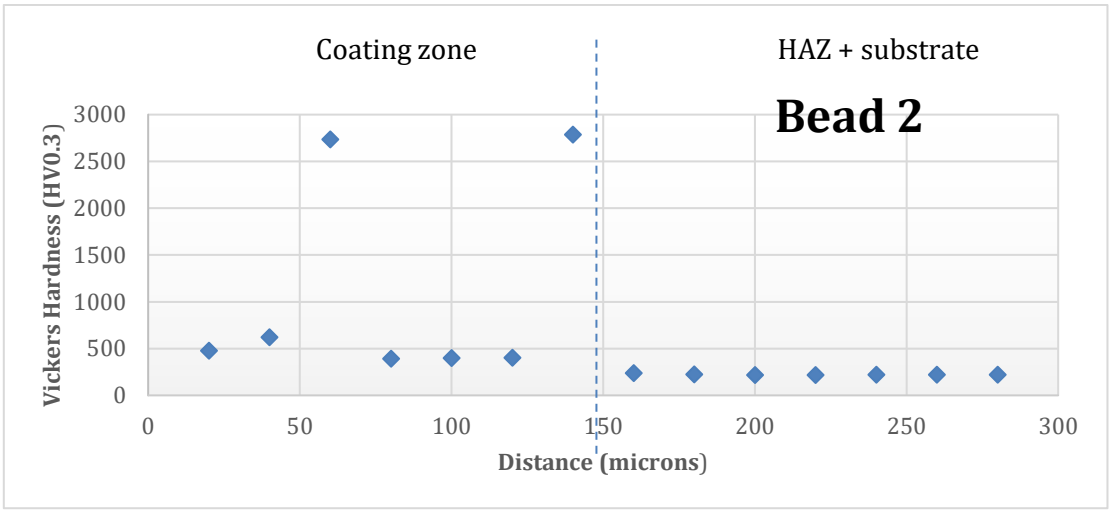
Coating zone
HAZ + substrate
Bead 2
Vickers Hardness (HV0.3)
3000
2500
2000
1500
1000
500
0
0
50
100
150
200
250
300
Distance (microns)

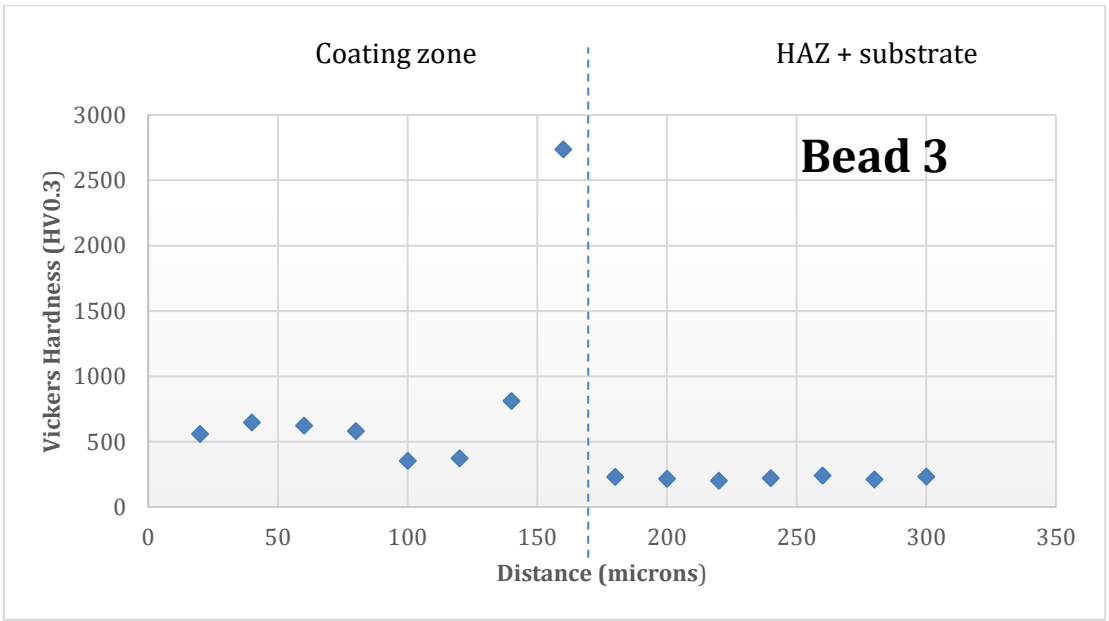
Coating zone
HAZ + substrate
Bead 3
Vickers Hardness (HV0.3)
3000
2500
2000
1500
1000
500
0
0
50
100
150
200
250
300
350
Distance (microns)

Sample 74

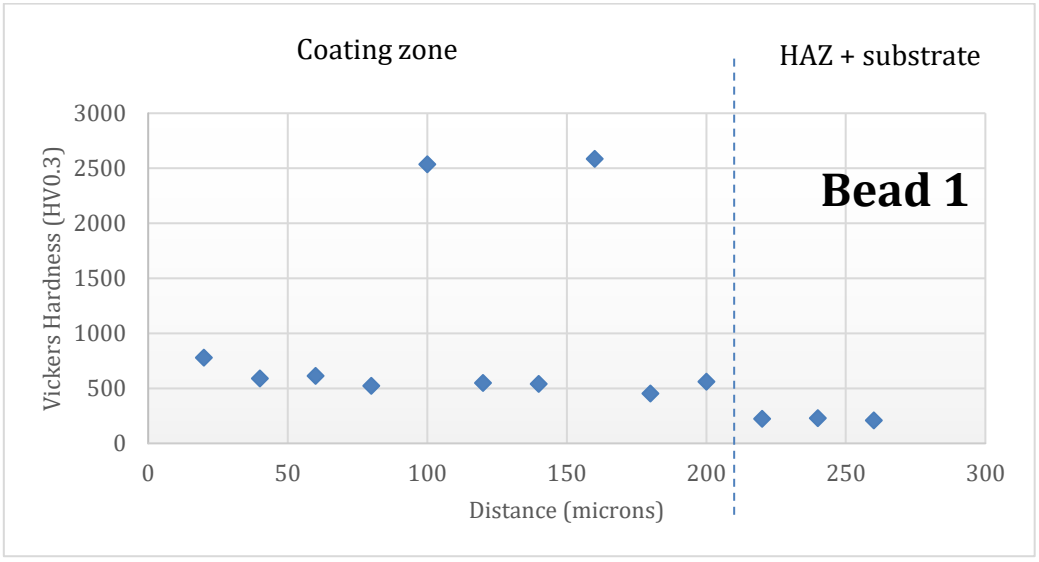
Coating zone
HAZ + substrate
Bead 1
Vickers Hardness (HV0.3)
3000
2500
2000
1500
1000
500
0
0
50
100
150
200
250
300
Distance (microns)

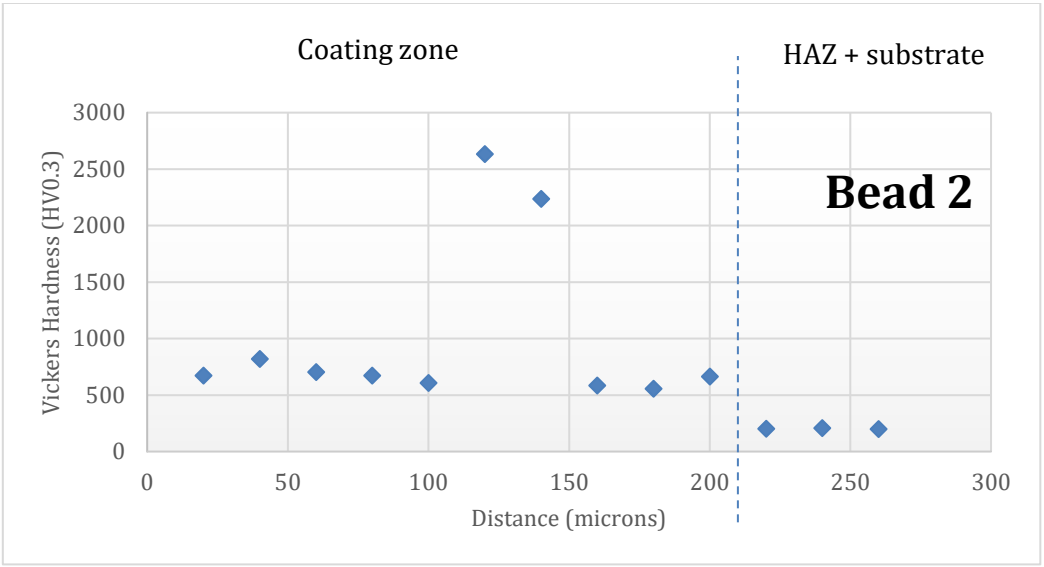
Coating zone
HAZ + substrate
Bead 2
Vickers Hardness (HV0.3)
3000
2500
2000
1500
1000
500
0
0
50
100
150
200
250
300
Distance (microns)

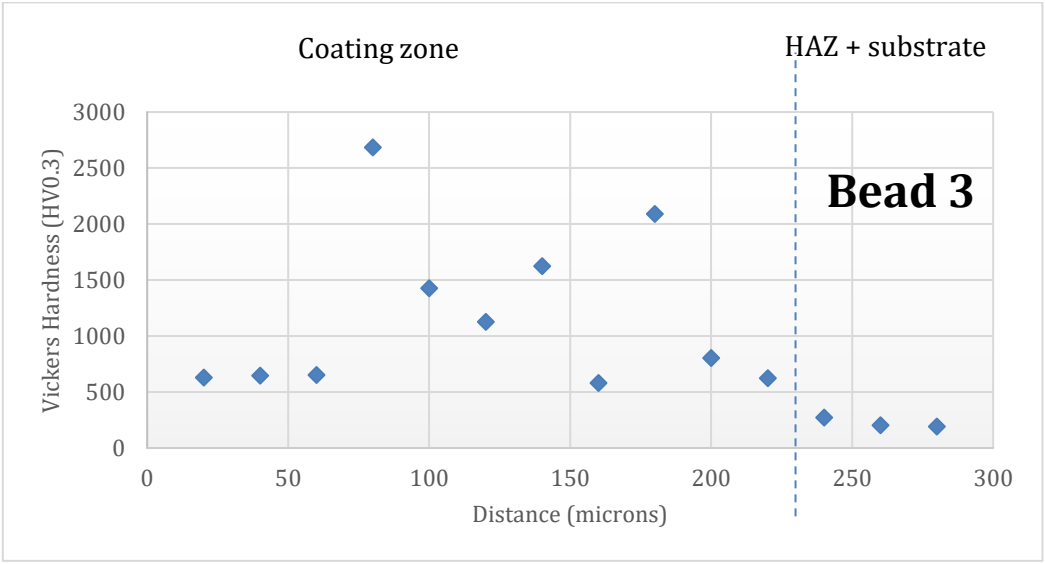
Coating zone
HAZ + substrate
Bead 3
Vickers Hardness (HV0.3)
3000
2500
2000
1500
1000
500
0
0
50
100
150
200
250
300
Distance (microns)